



STANFORD RESEARCH INSTITUTE
Menlo Park, California 94025 - U.S.A.

November 1, 1976

Quarterly Progress Report: PERC-0060-5
Covering the period 1 July to 30 September 1976

SULFUR POISONING OF CATALYSTS

By: W. E. Isakson, K. M. Sancier, H. Wise, and B. J. Wood

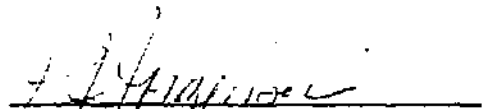
Prepared for:

U.S. ENERGY RESEARCH AND DEVELOPMENT ADMINISTRATION
Chicago Operations Office
9300 Cass Avenue
Argonne, Illinois 60439

Attention: Daryl B. Morse
Sr. Contract Administrator

Contract No. E(36-2)-0060
SRI Project 4387

Approved:


P. J. Jorgensen, Acting Director
Materials Research Center

NOTICE
This report was prepared as an account of work sponsored by the United States Government. Neither the United States nor the United States Energy Research and Development Administration, nor any of their employees, nor any of their contractors, subcontractors, or their employees, make any warranty, express or implied, or assume any legal liability or responsibility for the accuracy, completeness or usefulness of any information, apparatus, product or process disclosed, or represents that its use would not infringe privately owned rights.

MASTER

DISTRIBUTION OF THIS DOCUMENT IS UNLIMITED

CONTENTS

I	INTRODUCTION	1
II	SURFACE SULFIDATION AND SEGREGATION WITH METHANOL-SYNTHESIS CATALYSTS	2
	A. Experimental Program	2
	B. Experimental Results	2
	C. Discussion	3
	D. Conclusion	8
III	KINETICS OF CARBON FORMATION ON FISCHER-TROPSCH CATALYSTS	9
	A. Experimental Program	9
	B. Experimental Results	11
	1. Catalyst Reduction	11
	2. Thermomagnetic Analysis of Carbided Catalysts	12
	C. Discussion	13
	1. Reduction	13
	2. Carburization	15
	D. Conclusions	16
IV	PLANS FOR FUTURE WORK	17
V	REFERENCES	18

APPENDIX

I INTRODUCTION

This study, performed under ERDA Contract E(36-2)-0060, concerns the deactivation of catalysts used to produce fuels from carbon monoxide and hydrogen. The first phase of this research emphasized sulfur poisoning of methanol-synthesis catalysts. During this reporting period, we have begun to examine the role of carbon in Fischer-Tropsch catalysts. This report discusses surface sulfidation and segregation with methanol-synthesis catalysts (Section II), and the kinetics of carbon formation on Fischer-Tropsch catalysts (Section III). The thermodynamics and surface structures of sulfur chemisorbed on transition metals are reviewed in the Appendix.

II SURFACE SULFIDATION AND SEGREGATION WITH METHANOL-SYNTHESIS CATALYSTS

A. Experimental Program

To obtain quantitative data on the kinetics and mechanism of H_2S interaction with a methanol-synthesis catalyst (CCI C79-1), we have carried out a series of experiments by Auger electron spectroscopy (AES). The experimental apparatus, described in detail in our preceding quarterly progress report (PERC-0060-4), is essentially a nozzle-beam gas source pointing at a wafer of catalyst situated at the focal point of the Auger electron spectrometer. With this arrangement, the relative surface concentration of sulfur can be measured as a function of time while the catalyst is exposed to a known flux of hydrogen sulfide.

The catalyst sample was pretreated by heating it overnight in a stream of hydrogen at 525 K. Subsequently, it was mounted in the AES vacuum chamber and heated at 475 K in vacuum during an overnight bakeout. Base pressure in the vacuum chamber was maintained in the 10^{-9} torr range. During dosing of the catalyst surface, background pressures in the chamber reached about 5×10^{-8} torr. The gas flux from the nozzle at the specimen surface corresponded to a pressure of about 2×10^{-6} torr. In most experiments, the surface was dosed with a mixture of 1 vol% H_2S in H_2 .

B. Experimental Results

Since the low-pressure process for methanol synthesis is of primary industrial interest, we have concentrated our efforts on the copper-zinc-aluminum oxide catalyst formulation as exemplified by the CCI C79-1 catalyst. When this catalyst is exposed to a mixture of H_2S and H_2 ,

surface sulfur builds up until a steady-state saturation level is reached. These results (Figure 1) can be interpreted in terms of a kinetic model with first-order dependence on available adsorption sites and the H_2S pressure. For such a case, the following rate equation can be applied:

$$d\theta/dt = k(H_2S) (1 - \theta) \quad (1)$$

where θ represents the fraction of available adsorption sites occupied by sulfur, t is time, k is the reaction rate constant, and (H_2S) is the incident gaseous flux of hydrogen sulfide. If we assume that the observed sulfur saturation level corresponds to $\theta = 1$, we may integrate Equation (1) between the limits $\theta = 0$ at the onset and $\theta = 1$ at time t .

$$\ln(1 - \theta) = k(H_2S) t \quad (2)$$

Thus, for a specific constant flux of H_2S , the slope of a plot of $\ln(1 - \theta)$ against t is proportional to the rate constant, k . Our experimental data were analyzed in this way (Figure 2) and the values of k computed from the slopes and the H_2S dosing fluxes (Table 1).

C. Discussion

The AES measurements demonstrate that the rate of sulfur deposition on the surface of the C79-1 methanol-synthesis catalyst at 503 K exhibits a first-order dependency on the concentration of free surface sites and on the incident flux of hydrogen sulfide. Similar results were obtained with the catalyst at 300 K (Table 1). From the values of the rate constant measured at these two temperatures, we calculate an activation energy of 700 cal mol^{-1} .

Auger electron spectroscopy (AES) analyzes the elemental composition of a surface to a depth of less than 200 nm. However, the catalyst

wafers used in our studies were about 0.1 mm thick and contained considerable pore structure so that only a very small fraction of the total surface was examined by AES.

Under normal reaction conditions, gaseous molecules can enter the pores of a catalyst and react by collisional interaction with the interior walls of the pores. (At 500 psi, the average mean free path of an H_2S molecule is about 200 nm, comparable with the mean pore radius of typical oxide-based catalysts.¹) In contrast, under the conditions of our low-pressure experiments, multiple collision with the catalyst are unlikely, because the gaseous molecules emanating from the dosing nozzle enter a chamber at a background pressure about 10^{-7} torr where the average mean free path is about 10^9 nm. Consequently, saturation of the catalyst specimen with a sulfur adsorbate would represent full occupancy of the free sites on the outer surface of the catalyst only. The data obtained support this conclusion.

In our AES experiments with the C79-1 catalyst at 300 K, sulfur saturation was observed after the surface had been exposed to a cumulative dose of H_2S corresponding to 1.6×10^{16} molecules. From the measurements reported in the previous report (PERC 0060-4), we calculate a surface area of $5.4 \text{ m}^2 \text{ g}^{-1}$ for the ZnO component and $5.2 \text{ m}^2 \text{ g}^{-1}$ for the Cu component. Thus, for the mass of catalyst used in our low-pressure study (0.048 g), we arrive at a surface total site density of 2.5×10^{18} for each of these components--a number greater by a factor of 10^2 than that corresponding to the total H_2S exposure producing saturation surface coverage with sulfur. We conclude, therefore, that about 99 percent of the total active surface of the catalyst is to be found within the pore structure.

Mass transport can occur in adlayers by surface migration, and the rate of such a transport process is governed largely by the strength

of the adsorption bond and by the availability of free surface sites. In our experiments, the sulfur coverage on the outer surface of the catalyst was observed to diminish with time when the incident flux of H_2S was interrupted. In the range 300 to 473 K, the rate data (Table 2) yield an activation energy of $2300 \text{ cal mol}^{-1}$, a value of reasonable magnitude² for a surface migration process involving a species with a binding energy in the range 20 to 30 kcal mol^{-1} . Removal of a large fraction of the sulfur from the outer surface of a heavily dosed, saturated wafer at 503 K by argon ion bombardment (sputter etching) provided further evidence of the sulfur adspecies mobility. When the argon ion beam was interrupted, the sulfur concentration on the surface seen by AES slowly increased, evidently by surface migration of sulfur from within the pore structure.

Neither the chemical structure nor the distribution of the adlayer of sulfur on the C79-1 catalyst can be identified unequivocally from the AES data. To attempt to determine the location of the adsorbed sulfur species on the catalyst, we observed the rate of sulfur deposition on surfaces representative of the individual components of the catalyst, namely, ZnO, Cu, and Al_2O_3 . The existence of these specific phases in the reduced (activated) catalyst was inferred from data supplied by the manufacturer and from x-ray diffraction patterns obtained in our laboratory. For comparison purposes, we measured the rate of sulfur deposition on a Ni/ Al_2O_3 (25 wt% Ni) catalyst made from Girdler T-372 alumina (Table 1).

Zinc oxide, in striking contrast to the mixed oxide catalyst, exhibits no detectable sulfur accumulation when exposed to H_2S under our experimental conditions. On the basis of equilibrium data, ZnO should be readily converted to the sulfide in a gaseous environment of 1% H_2S in H_2 . Apparently, kinetic factors play a dominant role in this

reaction; multiple collisions of H_2S molecules on a ZnO surface are required to approach equilibrium conditions within a reasonable period of time.

The rate of sulfur accumulation on a copper surface is comparable to that measured for the methanol-catalyst surface. At 300 K, the sulfur adlayer on Cu is stable, as might be expected for a species chemisorbed on a metal surface. When the temperature is raised to 460 K, however, the concentration of surface sulfur increases slowly with time, suggesting the segregation of indigeneous bulk sulfur impurity to the metal surface.³ Deposits of sulfur on copper single crystals, exposed to hydrogen sulfide under conditions similar to our experiments, have been examined^{4,5} by low energy electron diffraction (LEED). The precise surface configuration assumed by the sulfur adspecies appears to depend on the magnitude of the incident H_2S flux and on the exposed crystal face. Within the H_2S pressure range of 10^{-9} to 10^{-5} torr, dissociative chemisorption occurs without surface reconstruction, leaving a sulfur adspecies that is free to migrate across the surface. Sulfur saturation corresponding to half a monolayer of adatoms was reported^{4,5} to require an exposure of approximately 10 Langmuir (10^{-5} torr sec.⁻¹), which is comparable to our experimental results (Figure 3).

The efficiency with which an H_2S molecule is dissociatively adsorbed on a clean copper surface is measured by the initial sticking probability, S_0 , defined as the ratio of the rate of interaction to the collision frequency:

$$S_0 = N(ds/dt)/Z \quad (3)$$

where N is the density of surface sites and Z , the incident flux of H_2S (molec $cm^{-2} min^{-1}$), is related to the H_2S pressure P :

$$P = Z(4RT/c) \quad (4)$$

In this expression, R is the gas constant ($\text{torr cm}^3 \text{ molec}^{-1} \text{ deg}^{-1}$), T is the gas temperature (deg K) and c is the mean velocity of the H_2S molecule (cm min^{-1}). At $\theta = 0$, the first-order rate law [Equation (1)] becomes

$$d\theta/dt = kP = kZ(4RT/c) \quad (5)$$

Therefore, combining Equations (3) and (5),

$$S_0 = Nk(4RT/c) \quad (6)$$

We observed that the rate of sulfur deposition on Cu follows first-order kinetics [Equation (1)]. Hence, for Cu foil with $N = 1.54 \times 10^{15}$ atoms cm^{-2} , $S_0 = 0.07$, that is, one in fifteen collisions results in adsorption of the H_2S molecule on the Cu surface.

Although in our low-pressure experiments H_2S adsorption on alumina can be demonstrated (Table 1), the interaction of H_2S with the alumina phase of the methanol catalyst is expected to be negligible under the conditions of methanol synthesis. Within the limit of AES detectability (approximately 0.05 monolayer), we found that H_2S would not adsorb on either of two types of alumina catalyst support unless the solid material was first heated in vacuum to about 825 K to expel strongly bound water. Others^{6,7} have reported small coverages of weakly bound H_2S on alumina and have suggested that the ad-molecule is hydrogen-bonded to the OH^- groups on the alumina surface. DeRossat et al.⁸ noted that the heat of adsorption of H_2S varied with the degree of predrying of the alumina, and suggested that the H_2S reacted as a base at Lewis acid sites on

dehydrated alumina. With the Kaiser alumina used in our experiments, we observed variations in the fine structure of the LVV lines in the Auger electron spectra. These variations accompanied dehydration and subsequent adsorption of H_2S . Specifically, an Auger line at 70 eV disappeared when the alumina specimen was heated to 800 K and subsequently cooled to 530 K in hard vacuum (approximately 10^{-8} torr). When the alumina specimen was exposed to H_2S (under the conditions previously described), the line reappeared in the spectrum and grew in intensity as the sulfur concentration on the surface increased. This behavior could be indicative of SH^- groups occupying sites on the dehydrated alumina surface in place of OH^- on the dehydrated surface. Species of this type are strongly bound.⁹

Our measurements indicate that the value of the rate of H_2S adsorption on dehydrated alumina is about one-third of that measured on the reduced mixed oxide catalyst (Table 1). However, under typical methanol synthesis conditions, the alumina phase present in the catalyst is likely to be unable to adsorb H_2S except in a weakly bound state at a very low degree of coverage.

D. Conclusion

Our sulfidation studies suggest that:

- H_2S dissociatively chemisorbs on the C79-1 catalyst surface to produce a surface-mobile sulfur adlayer.
- In low partial pressures of H_2S , the copper phase of the catalyst exhibits a high capture probability for H_2S and makes it highly susceptible to sulfur poisoning.

III KINETICS OF CARBON FORMATION ON FISCHER-TROPSCH CATALYSTS

A. Experimental Program

This study concerns the carbon build-up and removal from iron Fischer-Tropsch catalysts. During the current period, we have examined the kinetics of carbon formation and performed magnetic measurements to identify the iron carbide phases formed. The catalyst samples have been provided by ERDA-PERC and have been pretreated at SRI by reduction and carburization as directed by ERDA-PERC.

To study the magnetic properties of catalysts, we have constructed an apparatus incorporating a vacuum microbalance that can make simultaneous measurements of both the mass of a sample and its magnetic susceptibility. In this apparatus, the Faraday technique is used to measure the susceptibility, but the required vertical magnetic field gradient is provided by a set of electromagnetic coils rather than by a shaped pole face as previously used,^{10,11}

The schematic drawing of the apparatus in Figure 4(a) shows the main magnet. The hang-down tube communicates at one end with the balance and at the other end with a liquid nitrogen dewar for cooling the sample. The field gradient coils are affixed to the magnet pole faces. An enlargement of the apparatus in the pole-face region is shown in Figure 4(b). The field gradient coil provides a vertical magnetic field gradient that is linearly proportional to the current through the coils and is constant to $\pm 0.1\%$ over a vertical distance of 1 cm at the center where the sample is located. The hang-down tube is made of four concentric stainless steel tubes. The two inner tubes encase the sample and a thermocouple and provide a means for flow of various gases over

the sample. Between the second and third tubes is a space for controlling the sample temperature by an electric furnace capable of 925 K and by either cold gases or liquid nitrogen from the dewar below. The space between the third and fourth tubes is evacuated to decrease heat transfer from the sample area to the environment.

The field gradient coils provide a gradient that is independent of the main magnetic field, resulting in the following advantages over the usual Faraday method:

- The system is especially suitable for ferromagnetic samples.
- The contribution of ferromagnetism in diamagnetic and paramagnetic samples is easily eliminated.
- The components of force due to magnetism and sample weight are more easily distinguished, even when the sample mass is changing rapidly.
- The ability to rapidly reverse the field gradient eliminates zero point drift due to vibration and temperature changes. Moreover, the sensitivity is markedly increased by the use of signal averaging techniques, for example, lock-in detection at a constant current-reversing frequency.

A 20 to 35 \pm 0.05 mg sample of catalyst B6 (042175 AMRC-1) was weighed into a small quartz container and suspended from the Cahn microbalance. The sample was centered in the magnetic field gradient by maximizing the observed magnetization output. The entire system was purged with helium at 100 cm³ min⁻¹ for a minimum of 1 hour at 23°C. Hydrogen was then admitted at 100 cm³ min⁻¹, and the helium flow was discontinued to the portion of the apparatus having the sample. Helium flowed continuously through the Cahn microbalance case. After establishing

a temperature of 175°C, we programmed a temperature rise of 17°C hr⁻¹ to 450°C (about 16 hours). At the end of this period, the sample was cooled to room temperature in hydrogen. Temperature and sample mass were recorded throughout the reduction process.

Five carburization experiments were performed with Catalyst B6 after reduction in hydrogen. In the first of these, the temperature was set at 175°C and a H₂/CO flow was established (volume ratio = 3/1, flow rate 100 cm³ min⁻¹). The furnace was then programmed to provide a temperature increase of 63°C hr⁻¹ for 2 hours. After this time, the temperature was held at 300°C for 2 additional hours. In the other four experiments, the temperature was held constant over the entire period of carburization at 200°C, 250°C, 300°C, or 324°C. The CO used (Matheson "Ultra-pure" 99.8% CO) was further purified by passage through a copper tube packed with 1/8-inch Kaiser Al₂O₃ spheres and copper turnings and cooled in a bath of dry ice and acetone. Sample temperature and sample mass were monitored during the carburization process.

Samples carburized in situ were analyzed thermomagnetically immediately after carburization. The sample temperature was lowered from the carburization temperature at a rate of approximately 50°C min⁻¹ to about 150°C while an X-Y recorder monitored magnetization as a function of temperature. Subsequently, the temperature was raised at 25 to 50°C min⁻¹ to the desired maximum with recording of magnetization as a function of temperature.

B. Experimental Results

1. Catalyst Reduction

In hydrogen, no weight loss of catalyst B6 was detectable at temperatures below 260°C. In the 6 hours during which the temperature

was raised to 400°C, all samples lost $21.3 \pm 0.1\%$ of their initial mass. No further weight loss occurred in the following 2 hours during which the temperature was raised slowly to 450°C in hydrogen.

A thermomagnetic analysis (TMA) obtained for the unreduced catalyst is shown in Figure 5. Two major ferromagnetic components were observed, one with a Curie temperature of 561°C, the other with a Curie temperature of 235°C. The residual magnetism at 650°C is due to a third ferromagnetic component with a Curie temperature greater than 650°C. The total time for the thermomagnetic analysis from room temperature to 650°C was 20 minutes. In the temperature-programmed carburization study, catalyst B6 exhibited the mass changes listed in Table 3. The results of the carburizations performed at constant temperature (200°C, 250°C, 300°C, and 324°C) are summarized in Table 4. Figure 6 is a plot of the mass change as a function of carburization time at 250°C. The curve shown, typical of all four isothermal carburization experiments, an initial rapid rate of mass gain is followed by a somewhat slower rate. The rates of mass gain in the initial and in the subsequent stages are compiled in Table 4. The table also lists the time, t_p , at which transition occurs between the high and low rates of mass change (Figure 6).

2. Thermomagnetic Analysis of Carbided Catalysts

Thermomagnetic analyses (TMA) were performed on each of the carbided samples of Catalyst B6 immediately after carburization. The results of a TMA with decreasing and increasing temperature are shown in Figure 7. The two curves show a small difference in Curie temperature (about 5°C) which is probably due to a thermal gradient between the sample and the thermocouple during the temperature-programmed measurements. Based on the exhibited values for the Curie temperatures of various phases to be found in iron-based Fischer-Tropsch catalysts (Table 5) we have

interpreted the Curie temperatures observed in our carburization studies in terms of ferromagnetic phases (Table 6).

To confirm these assignments of the Curie temperatures, we heated some samples of Catalyst B6 briefly (3 to 12 minutes) in hydrogen to higher temperatures at which known bulk phase transformations occur. Samples exhibiting an original Curie temperature of 330°C to 365°C* (hexagonal Fe_2C) were transformed to a material with a Curie temperature of about 245°C (Hagg) when heated to temperatures above 350°C. Samples with an original Curie temperature of about 245°C (Hagg) were transformed to a material with a Curie temperature of about 219°C when heated to above 500°C (cementite, Fe_3C).

In a separate experiment, a sample carburized at 324°C was analyzed by TMA after 8 minutes of carburization and a 0.75-mg mass gain. This analysis in the direction of decreasing temperature (Figure 8, dashed curve) indicates the formation of a small amount of a material with a 245°C Curie temperature (Hagg). After further carburization until the mass gain was approximately doubled (1.4 mg), the sample was again analyzed by TMA (Figure 9, solid curve). The results suggest that the amount of ferromagnetic material with a Curie temperature of 245°C increases twice as fast as the mass of the sample.

C. Discussion

1. Reduction

The Fe^{2+} and Fe^{3+} concentrations indicated by chemical analysis¹² of Catalyst B6 suggest the predominance of stoichiometric Fe_3O_4 (plus approximately 1.3% promoters) in the sample. For complete reduction of

*The hexagonal Fe_2C transforms to the Hagg carbide above 320°C, so that the apparent Curie temperature depends on the rate of temperature increase during thermomagnetic analysis.

Fe_3O_4 to Fe, a mass loss of 27.5% is expected. In our experiments, we observed a weight loss of 21.3% during reduction, indicating that either the catalyst cannot be reduced completely, or iron-containing phases other than Fe_3O_4 are present in the as-received sample.

Information on the identity and approximate amounts of the ferromagnetic phases were obtained by TMA. The TMA of the as-received catalyst before reduction shows that the major component has a Curie temperature of 561°C , which is probably due to $\gamma\text{-Fe}_3\text{O}_4$ (see Table 5). To account for residual magnetization above this temperature, a ferromagnetic phase must be present with a Curie temperature above 650°C (the maximum temperature we could attain), and this phase could be either Fe_2O_3 or $\alpha\text{-Fe}$, with Curie temperatures of 675 and 768°C respectively. The thermomagnetic curve near 650°C is nearly flat, which suggests that a component with a Curie temperature of 675°C (Fe_2O_3) is probably absent. Furthermore, the iron-oxygen phase diagram indicates that below 580°C for an oxygen content of 21.3%, the stable phases are primarily $\alpha\text{-Fe}$ + magnetite ($\gamma\text{-Fe}_3\text{O}_4$). Thus, we conclude that the major components of this unreduced catalyst are $\gamma\text{-Fe}_3\text{O}_4$ and $\alpha\text{-Fe}$. The minor component with the Curie temperature of 235°C has not yet been identified. It could be associated with an iron carbide, perhaps the Hagg carbide, present as small crystallites (domains), which would cause Curie temperature to decrease from the normal value of 247°C .

The mass fraction of ferromagnetic components in the sample can be estimated from the measured values of saturation magnetization and molecular weight. By such an analysis, we estimate that the $\gamma\text{-Fe}_3\text{O}_4$ content is about 80 to 85%. This value is in satisfactory agreement with the result obtained from weight changes during reduction, from which we calculated that the as-received catalyst contained 77% $\gamma\text{-Fe}_3\text{O}_4$. The remainder is $\alpha\text{-Fe}$, promoters, and possibly some iron carbide.

2. Carburization

During the temperature-programmed carburization study, a nearly constant rate of mass increase was observed as the sample temperature was increased from 200°C to 300°C. These data suggest that the apparently low activation energy for the rate-limiting step could be the result of a diffusion-controlled process. If the carburization rate at constant temperature is limited by diffusion in the solid phase, then the mass increase should follow a parabolic rate law, $M = \sqrt{cDt}$ where M is the mass, c is a proportionality constant, D is the diffusion coefficient, and t is the time. To test this hypothesis, we have analyzed our experimental results in terms of the mass increase, as a function of the square root of time for the isothermal carburization (Figure 9). A mass increase of 10.7% is required to produce stoichiometric Fe_2C from pure iron. If other carbon-containing products, such as graphite or wax, are formed, a mass increase of more than 10.7% is required. Our carburization experiments were discontinued before this value was reached. The family of curves at the four carburization temperatures suggests the existence of two diffusion-controlled regimes. In addition, the transition from one regime to the other appears to be temperature-dependent. By analyzing the rates in terms of the Arrhenius equation (Figure 10) we evaluated the activation energy. During the initial carburization stage, its value is 9.5 kcal mole⁻¹. In the subsequent stage its value is 6.5 kcal mol⁻¹.

Existence of two distinct phases for the carburization process may be interpreted in terms of formation of a precursor carbide in which diffusion is fast, and later transformation into a stable carbide in which diffusion is slow. The TMA results support the possibility of the formation of a precursor carbide (Figure 8). In the initial stage of carburization, we observe only a small amount of a ferromagnetic phase attributable to Hagg carbide; the remainder of the magnetization

results from α -Fe and perhaps some other carbide such as the hexagonal Fe_2C . In the later stage of carburization, the TMA results indicate an increase in the amount of Hagg carbide by more than a factor of 4, although the mass change is less than a factor of 2. Evidently, the carbon added to the catalyst during the initial stage does not produce much Hagg carbide. Also, it is possible that the carbide grains formed during the initial carburization stage are too small to be ferromagnetic.

The character of the ferromagnetic phases produced by carburizing Catalyst B6 in a H_2/CO mixture depended strongly on the temperature of carburization. Carburization at 300°C and 324°C produced the Hagg carbide, carburization at 250°C produced a mixture of Hagg and hexagonal Fe_2C , and carburization at 200°C produced only the hexagonal Fe_2C .

D. Conclusions

Several iron-based Fisher-Tropsch catalysts were examined during reduction and carburization by thermogravimetric (TGA) and thermomagnetic (TMA) analyses. Catalyst B6 was reduced in hydrogen and carburized in $\text{H}_2/\text{CO} = 3$ at atmospheric pressure. The results indicate that the fresh catalyst contains 77 wt% $\gamma\text{-Fe}_3\text{O}_4$, the remainder is $\alpha\text{-Fe}$, promoters, and possibly, some carbidic compounds. Carburization carried out under temperature programming conditions in the range of 175°C to 324°C results in the formation of Hagg carbide, Fe_2C , as the only ferromagnetic phase. Carburizations performed isothermally indicate the formation of: Hagg carbide at 300°C and 224°C , a mixture of Hagg and hexagonal Fe_2C at 250°C , and hexagonal Fe_2C at 200°C . Formation of a precursor carbide is suggested during early stages of carburization at 324°C .

The TGA results indicate the existence of two successive diffusion-limited carburization rates. From the temperature dependence of these two rate processes, the isothermal work of diffusion was calculated to be 9.5 and 6.5 kcal mol⁻¹.

IV PLANS FOR FUTURE WORK

Since copper apparently plays a key role in the H_2S poisoning of the low-pressure-process methanol-synthesis catalysts, it is of interest to evaluate the effect of copper concentration on the sulfur deposition rate. We plan to continue our AES studies with a wafer of catalyst "B", which contains a considerably higher ratio of Cu/ZnO than the C79-1 catalyst. In addition, we will examine the rate of sulfur deposition on a zinc chromite high-pressure-process catalyst that contains no copper.

In further studies of carbon formation on iron Fischer-Tropsch catalysts, we will investigate the existence of a precursor carbide that may be formed during carburization and the influence of H_2/CO ratio on the character of the carbides formed during carburization. Carburization rates and thermomagnetic properties, will be investigated for several other catalysts provided by ERDA/PERC.

V REFERENCES

1. S. J. Gregg and K.S.W. Sing, "Adsorption, Surface Area and Porosity", (Academic Press, New York, 1967), p. 166.
2. J. W. Geus, in "Chemisorption and Reactions on Metallic Films", J. R. Anderson, editor, (Academic Press, New York, 1971), Chapter 3.
3. R. W. Joyner, C. S. McKee and M. W. Roberts, Surface Sci., 26, 303 (1971).
4. J. Benard, Catalysis Rev. 3, 93 (1969).
5. R. W. Joyner, C. S. McKee and M. W. Roberts, Surface Sci., 27, 279 (1971); H. P. Bonzell, Surface Sci., 27, 387 (1971).
6. A. V. Deo, I. G. Dalla Lana, and H. W. Habgood, J. Catalysis, 21, 270 (1971).
7. R. W. Glass and R. A. Ross, J. Phys. Chem., 77, 2576 (1973).
8. A. J. de Rosset, C. G. Finstrom, and C. J. Adams, J. Catalysis, 1, 235 (1962).
9. J. B. Peri, J. Phys. Chem., 69, 211 (1965).
10. R. T. Lewis, Rev. Sci. Instr., 42, 31 (1971).
11. R. T. Lewis, J. Vac. Sci. Technol., 11, 404 (1974).
12. Memo to B. B. Blaustein, PERC from J. E. Mauser, Bu. of Mines, Albany Metallurgy Research Center, April 18, 1975.
13. W. Jost, "Diffusion in Solids, Liquids, Gases," (Academic Press, New York, 1952), p. 344.
14. H. H. Storch, N. Columbic, and R. B. Anderson, "The Fischer-Tropsch and Related Syntheses," John Wiley and Sons, Inc., New York 1951.
15. E. M. Cohn, E. H. Bean, M. Mentser, L.J.E. Hofer, A. Pontello, W. C. Peebles, and K. H. Jacks, J. Appl. Chem., 5, 418 (1955).

16. H. Pichler and H. Merkel, "Chemical and Thermomagnetic Studies on Iron Catalysts for Synthesis of Hydrocarbon," U.S. Bureau of Mines, Technical Paper 718, (1949).
17. E. C. Stoner, "Magnetism and Matter," (Methuen and Co., London, 1934), pp. 280-434.

Table 1

SULFIDATION RATE CONSTANTS FOR CATALYSTS AND CATALYST
COMPONENTS DETERMINED BY AUGER ELECTRON SPECTROSCOPY

Specimen ^a	Temperature (K)	Rate Constant k (Eq. 1) (torr min) ⁻¹ x 10 ⁻⁵
C79-1	300	9.6
	503	13.8 ± 0.5
Al ₂ O ₃ (Girdler T-372) ^b	488	3.1 ± 0.2
Al ₂ O ₃ (Kaiser) ^b	488	2.7
Cu (foil)	300	10.2
ZnO	300	0
	503	0
Ni/Al ₂ O ₃ (Girdler G65)	553	6-9

^aWith the exception of the Cu foil, all specimens were thin wafers pressed from powdered material.

^bDehydration in vacuum at T ≈ 825 K was required before sulfur-uptake was observed.

Table 2

SURFACE MIGRATION RATE OF SULFUR ON C79-1 CATALYST
AS MEASURED BY AUGER ELECTRON SPECTROSCOPY

Temperature	Rate of S Loss from Outer Surface (% min ⁻¹)
300	0.02
373	0.07
473	0.12

Table 3

TEMPERATURE-PROGRAMMED* CARBURIZATION
EXPERIMENT WITH CATALYST B6 (04 2175 ANRC-1)

Time (min)	Temperature (°C)	$\Delta m/\Delta t$ (mg hr ⁻¹)	Δm (mg)
0-30	175-200	0.15	0.80
30-140	200-300	0.45	} 1.05
140-180	300	0.45	
180-240	300	0.15	0.15

* Linear rate of temperature rise of 63°C hr⁻¹.

Table 4

CARBURIZATION RATES FOR CATALYST B6

Expt. No.	Carburization Temperature ^a (°C)	Weight of Reduced Catalyst (mg)	Rate of Mass Increase		τ_b (min)
			Initial Stage ^b (mg min ⁻¹) $\times 10^2$	Later Stage ^b (mg min ⁻¹) $\times 10^3$	
620-10	324	29.70	9.8	12.8	8
620-3	300	26.90	7.3	11.0	10
620-6	250	24.50	3.3	3.0	25
620-8	200	21.19	0.95	1.7	55

^a Carburization in H₂/CO = 3 flowing at 100 cm³ min⁻¹ at atmospheric pressure.

^b See Figure 6 and text for explanation.

Table 5

CURIE TEMPERATURES OF FERROMAGNETIC PHASES
PRESENT IN FISCHER-TROPSCH CATALYSTS

Phase	Curie Temperatures (°C)	Reference
α -Fe	768	14
Fe_2C , hexagonal	380	14
Fe_2C , Hagg	247 to 265 ^a	14
	276	15
Fe_3C , cementite	210	14
	205 to 220	16
Fe_3O_4 , magnetite	565	14
	580 to 595	17
α - Fe_2O_3 , cubic	500, 600, 650, 675	16
	675	17
α - Fe_2O_3	b,c	
Fe OOH	b	
$\text{K}_2\text{O}\cdot\text{Fe}_2\text{O}_3$, potassium ferrite	150	14
$\text{CuO}\cdot\text{Fe}_2\text{O}_3$, copper ferrite	450	14

^a Stable form

^b Paramagnetic only

^c Weakly ferromagnetic

Table 6

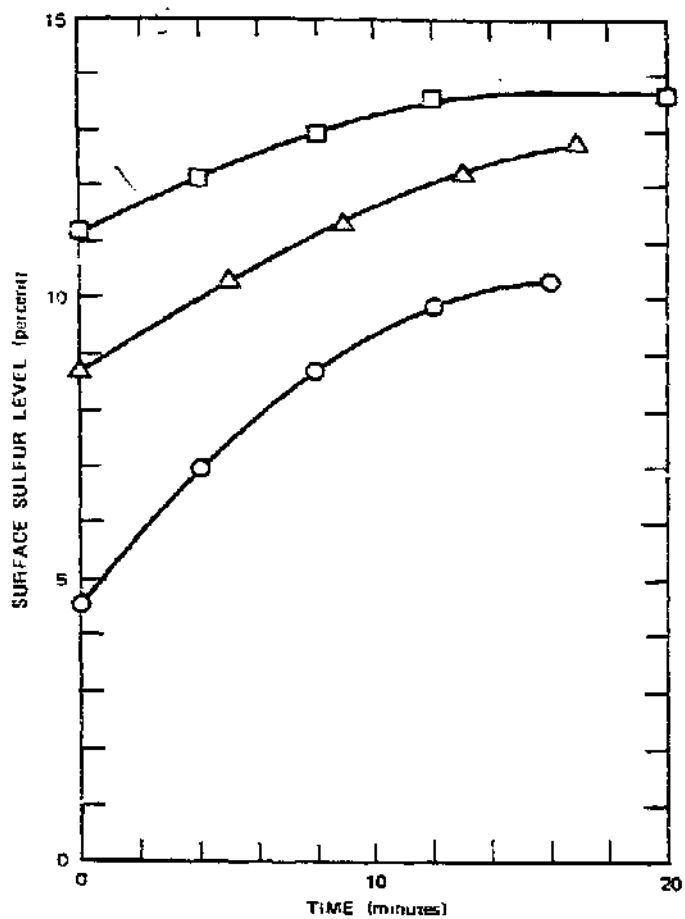
CURIE TEMPERATURES OBSERVED IN CATALYST B6 WHEN
CARBURIZED IN $H_2/CO = 3$ AT ATMOSPHERIC PRESSURE

Experiment No.	Carburization Temperature (°C)	Observed Curie Temperatures ^b (°C)	Probable Ferromagnetic Phases
620-1	175 to 300 ^a	247 525 ^c > 600 ^c	Hagg - α -Fe
620-10	324	245 > 324 ^c	Hagg α -Fe
620-3	300	247 > 560 ^c	Hagg α -Fe
620-6	250	248 > 365	Hagg (hexagonal Fe_2C α -Fe
620-8	200	330 > 445	hexagonal Fe_2C α -Fe

^aTemperature programmed at $63^\circ C \text{ hr}^{-1}$

^bThe (>) notation indicates maximum temperature of thermomagnetic scan; the residual magnetization at this temperature is an indication of the ferromagnetic phase which may have a higher Curie temperature.

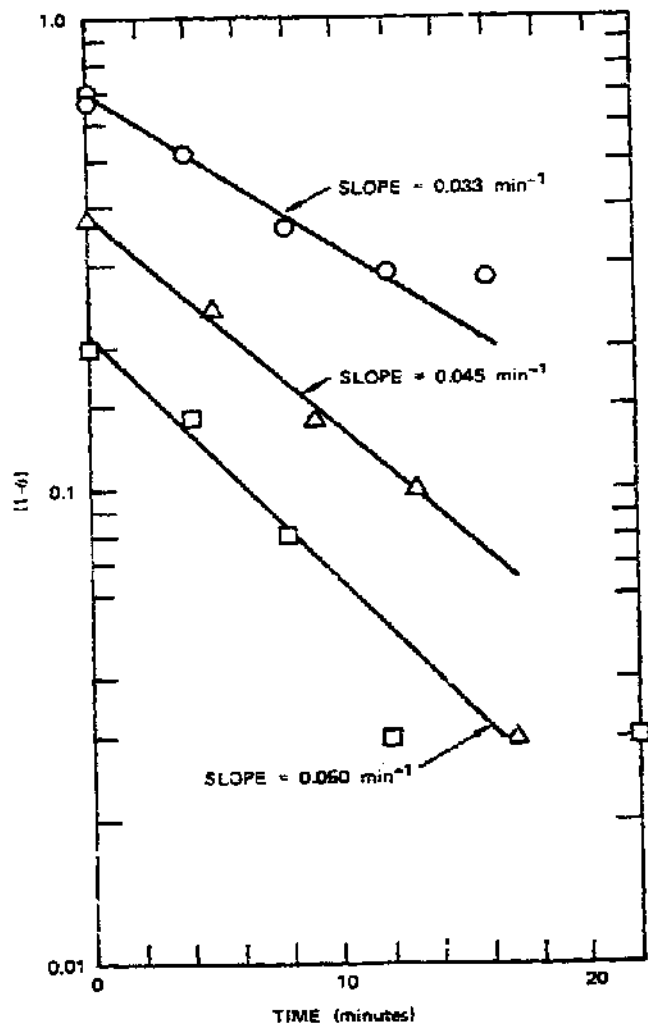
^cMinor constituent.



SA-4337-23

FIGURE 1 SULFUR DEPOSITION ON SURFACE OF C78-1 CATALYST WAFER DURING EXPOSURE TO H₂S

H₂S flux (expressed as equivalent pressure in torr x 10⁵):
 ○ 5.3; △ 7.8; □ 8.4. Temperature: 503 K.



SA-4387-24

FIGURE 2 DIMINUTION IN FRACTION OF AVAILABLE ADSORPTION SITES $(1-\theta)$ ON C79-1 CATALYST WAFER DURING EXPOSURE TO H_2S $P_{\text{H}_2\text{S}}$ (torr $\times 10^2$): \circ 5.3; Δ 7.8; \square 8.4. Temperature: 503 K.

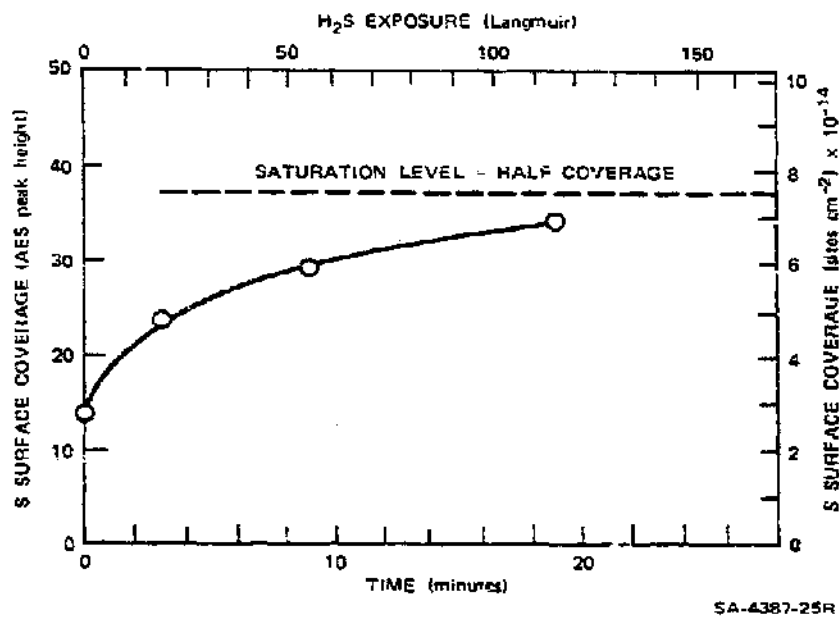
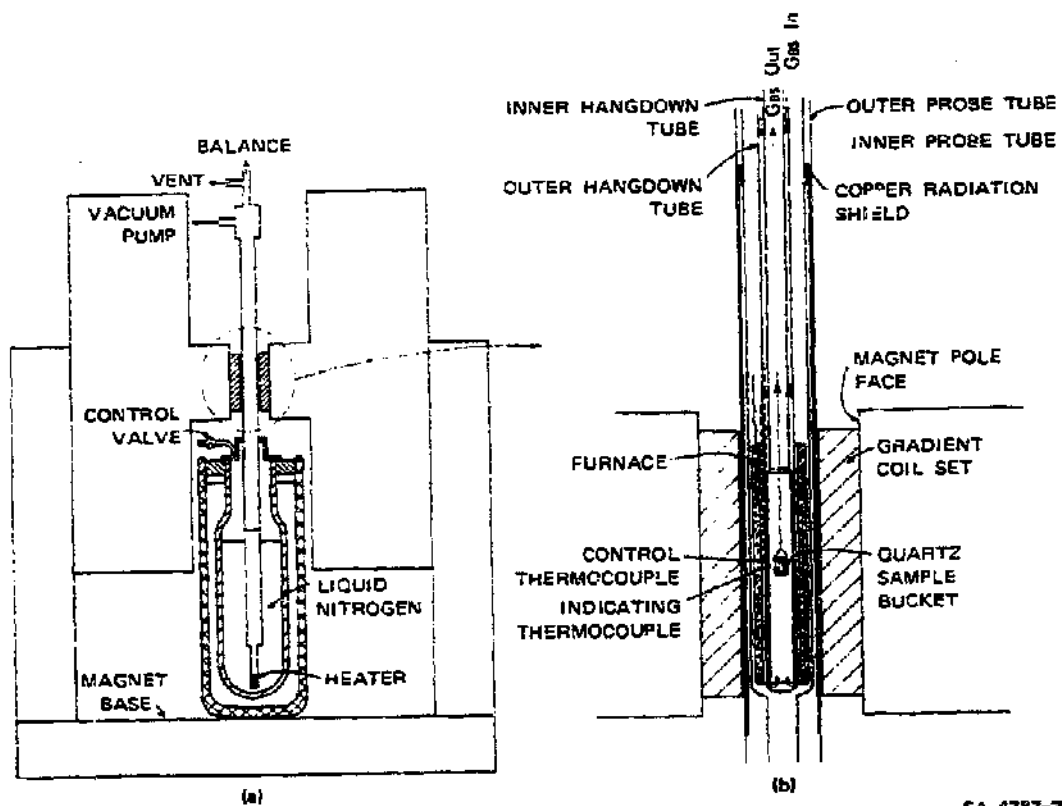


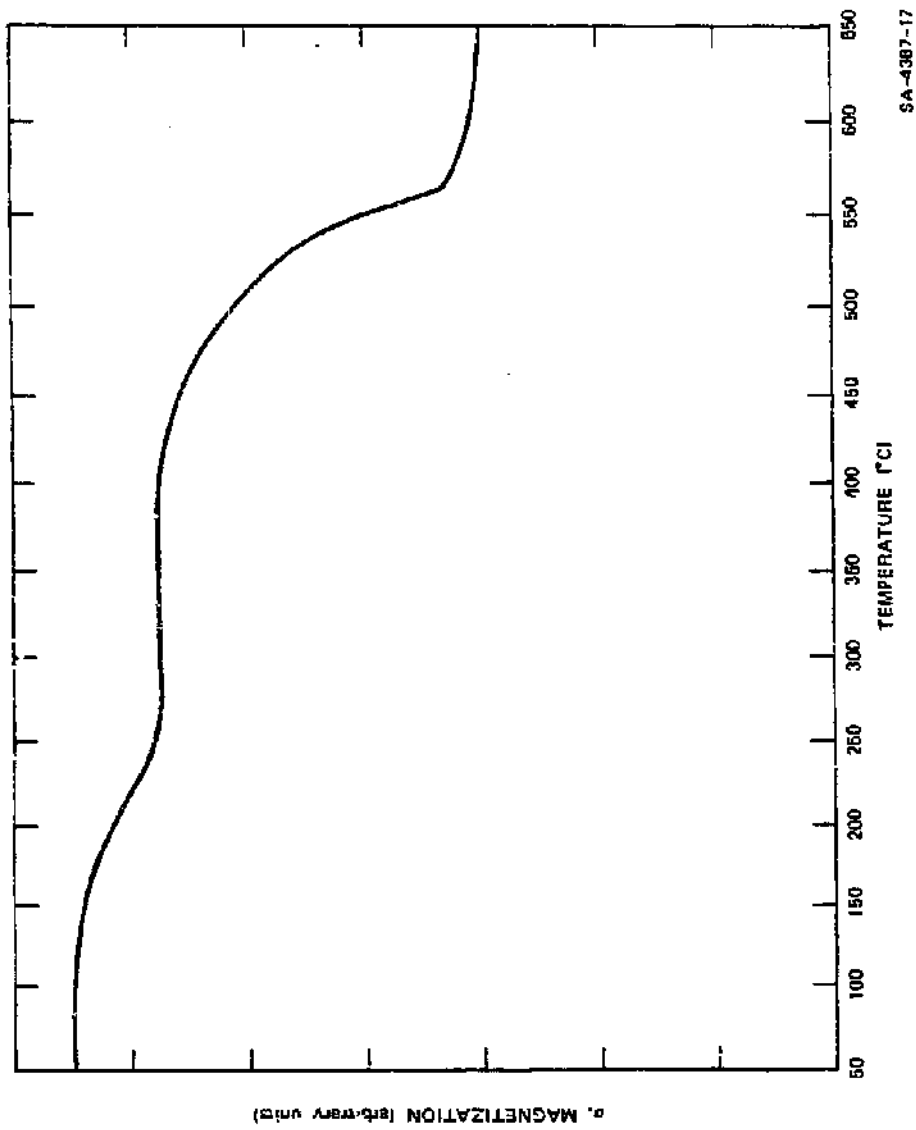
FIGURE 3 SULFUR DEPOSITION ON COPPER FOIL SURFACE EXPOSED TO H₂S

H₂S flux: 1.9×10^{16} molec min⁻¹ cm⁻² ($\equiv 8.9 \times 10^{-7}$ torr).
 Temperature: 300 K.



SA-4287-29

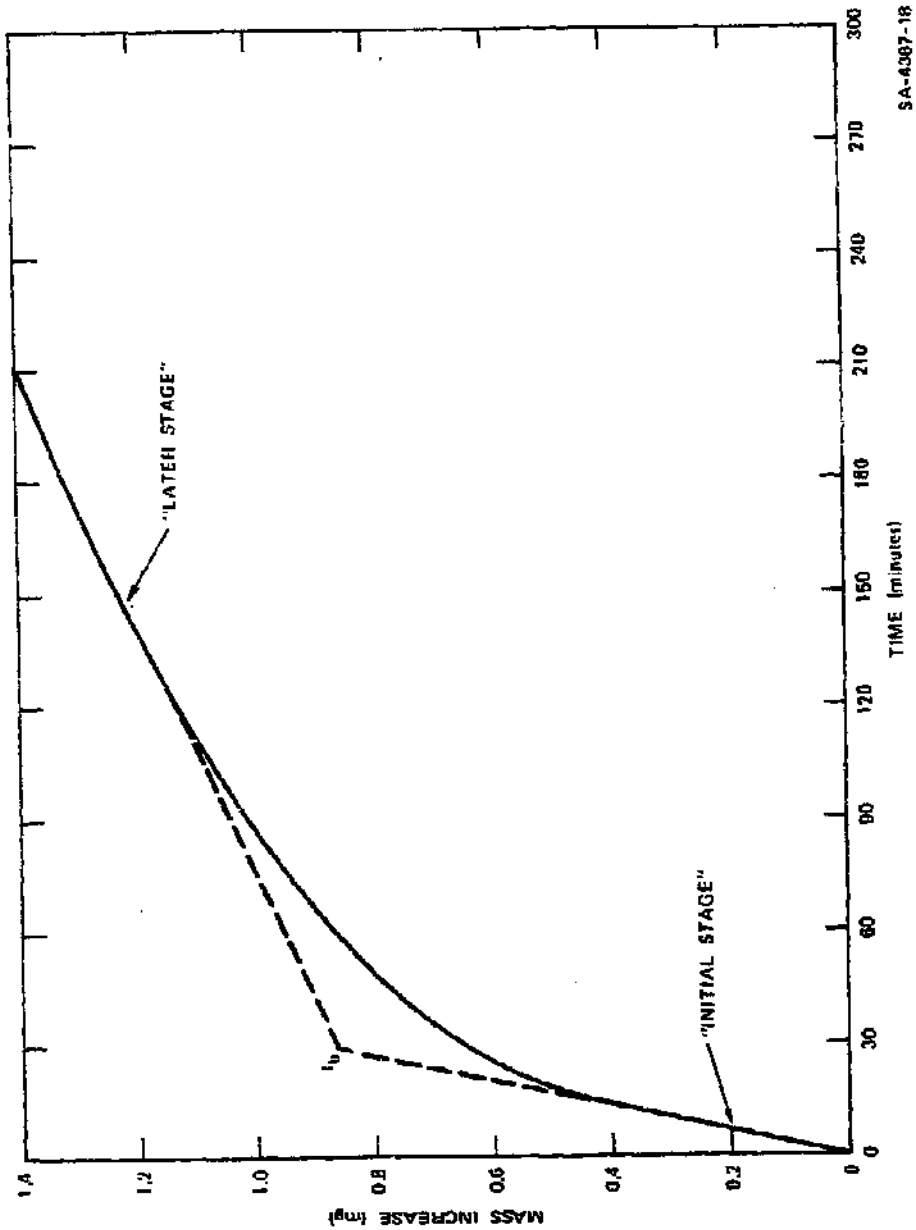
FIGURE 4 SCHEMATIC OF FARADAY TYPE MAGNETOMETER WITH ADJUSTABLE FIELD-INDEPENDENT GRADIENT AND VARIABLE TEMPERATURE PROBE
Over-all apparatus shown in (a) and enlargement of sample area shown in (b).



SA-4387-17

FIGURE 5 THERMOMAGNETIC ANALYSIS OF UNREDUCED CATALYST B8

Sample mass = 28.80 mg; magnetic field = 2.0 kgauss;
rate of heating = 30°C min⁻¹.



SA-4367-18

FIGURE 6 MASS INCREASE DURING CARBURIZATION OF CATALYST B6
 $H_2/CO = 3$; temperature = $250^\circ C$; sample mass = 24.50 mg.

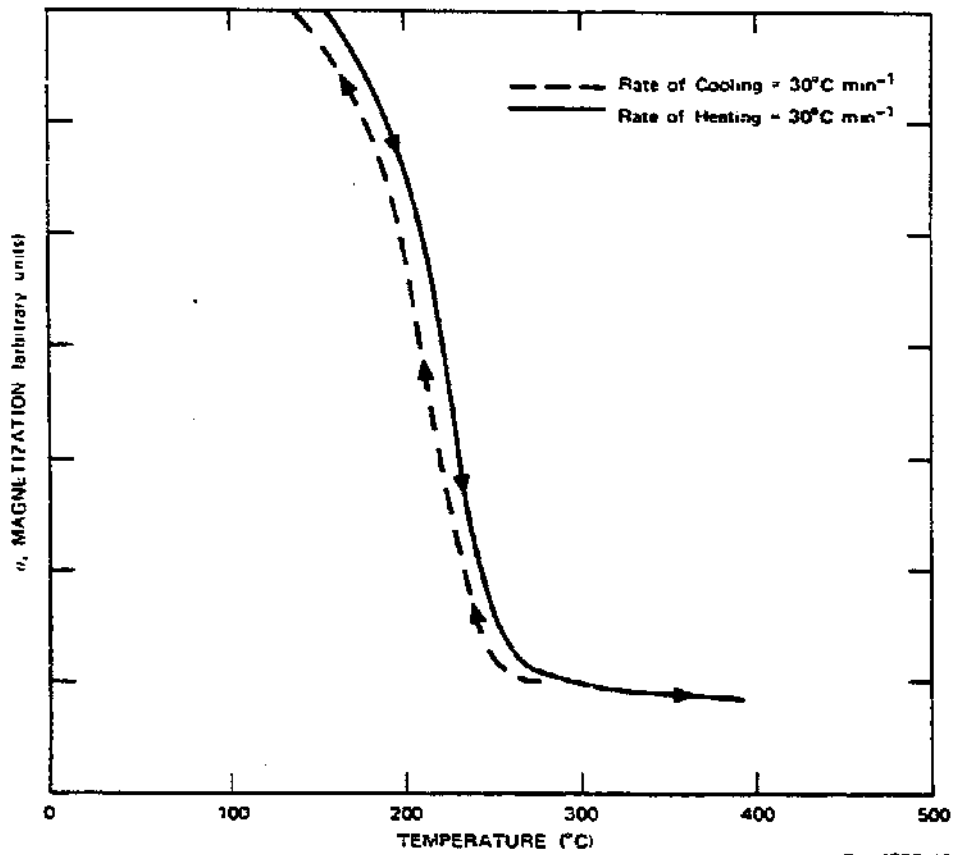


FIGURE 7 THERMOMAGNETIC ANALYSIS OF CATALYST B6 AFTER CARBURIZATION
 IN $H_2/CO = 3$ AT 300°C
 Magnetic field = 2.0 kgauss.

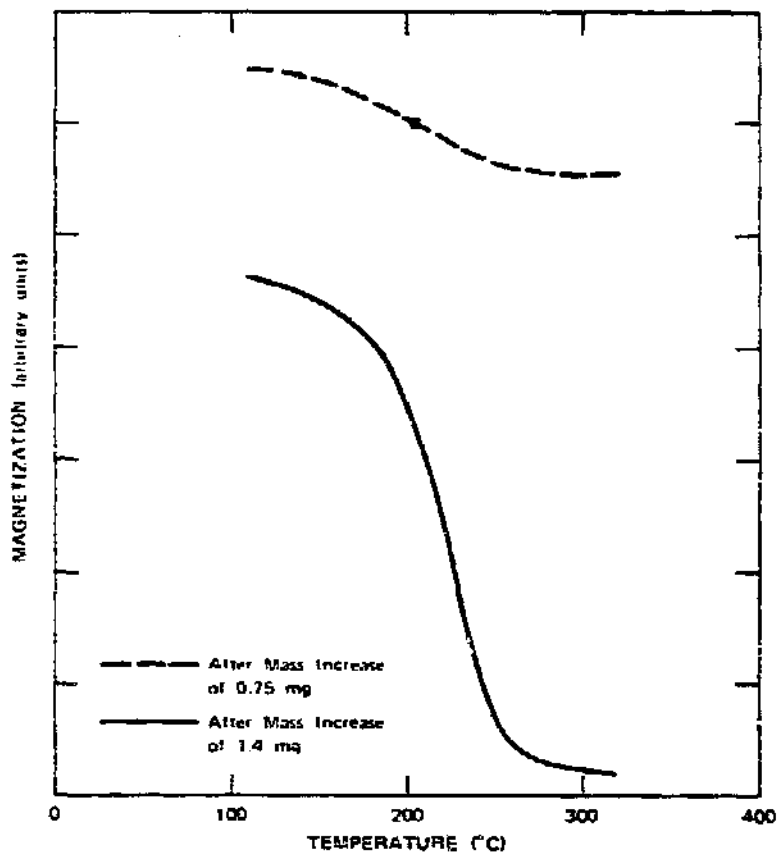
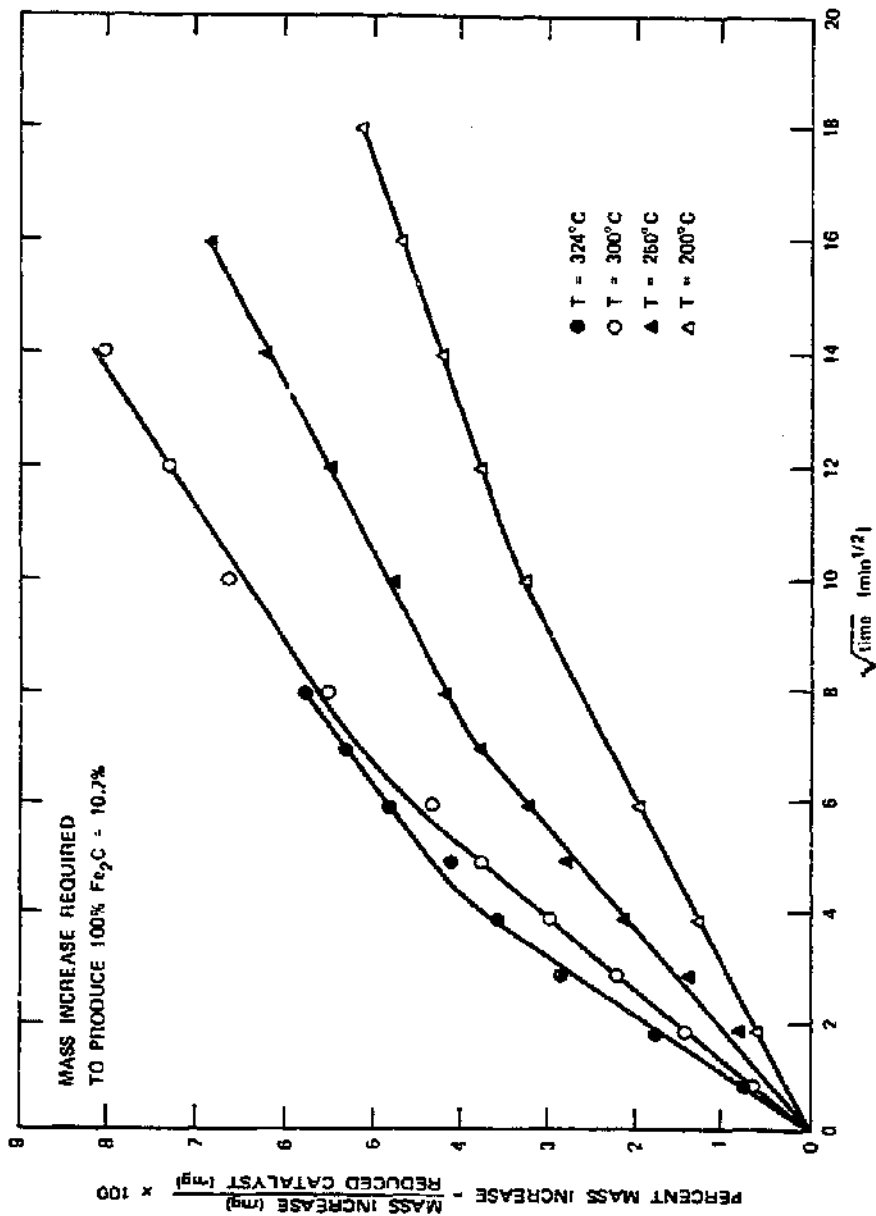


FIGURE 8 THERMOMAGNETIC ANALYSIS OF CATALYST 86 DURING CARBURIZATION IN $H_2/CO = 3$ AT $324^\circ C$

Magnetic field = 2.0 kgauss; rate of cooling = $30^\circ C$ min;
 sample mass = 29.70 mg after reduction.



5A-4387-71

FIGURE 9 CARBURIZATION OF CATALYST B6

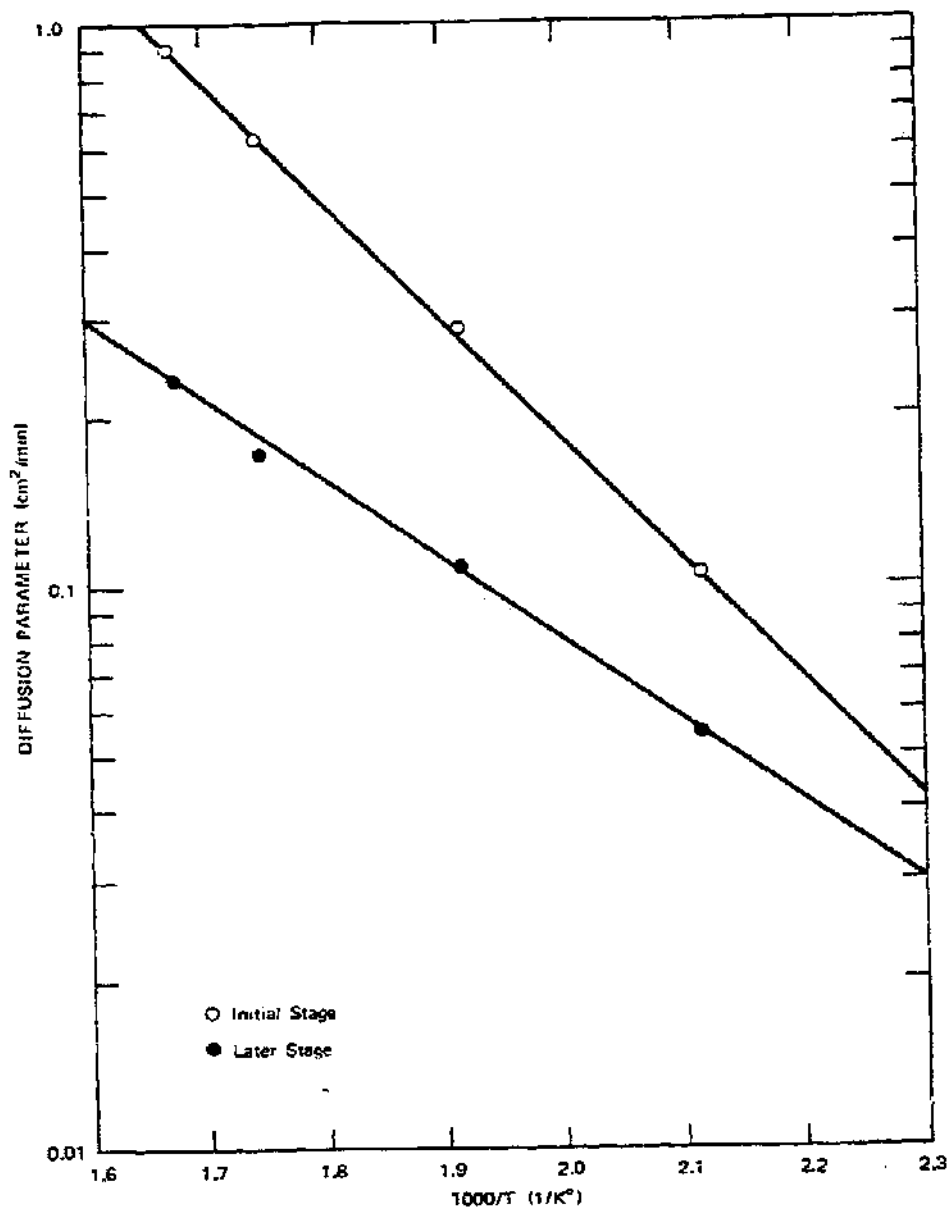


FIGURE 10 ARRHENIUS PLOT OF DIFFUSION PARAMETER FOR CARBURIZATION OF CATALYST B6

The diffusion parameter is equal to the square of the slopes of the curves in Figure 9.

APPENDIX

THERMODYNAMICS AND SURFACE STRUCTURES OF SULFUR CHEMISORBED ON TRANSITION METALS

Jon G. McCarty

Introduction

Catalyst poisoning by sulfur is a major problem in processes designed to convert synthesis gas into high Btu products, for example, methane, gasolines, or methanol. The sulfur tolerance limits necessary to attain reasonable catalyst life are typically set at about 0.1 ppm H_2S (or equivalent organic sulfur) for nickel methanation catalysts,¹ 0.03 ppm for iron Fischer-Tropsch catalysts,¹ and 1 ppm for copper/zinc oxide methanol synthesis catalysts.² Clearly, there is economic incentive to develop catalysts that have a higher sulfur tolerance or can be easily and inexpensively regenerated.

To gain an understanding of the reasons why sulfur is such an effective poison and why it is so difficult to remove chemisorbed sulfur from Ni, Fe, and Cu metal surfaces, we have reviewed research performed during the past 10 to 15 years concerning the thermodynamics and structure of sulfur adsorption on these metals. Specifically, the paper discusses the equilibrium thermodynamics and kinetics of adsorption/desorption of chemisorbed sulfur, the surface structure of bound sulfur, and the growth rates and thermodynamics of bulk metal sulfides.

Bulk Metal Sulfides

The thermodynamics and phase diagrams of bulk Ni, Fe, and Cu sulfides are relatively well documented. The nickel-sulfur phase diagram as represented by Figure 1 shows many phase transitions and bulk phases,³ for example, below 773 K, Ni_3S_2 is the most stable phase (i.e., the first to precipitate). The Ni-S thermodynamic data⁴ are

plotted as sulfur activity, defined by the partial pressure ratio, $P_{\text{H}_2\text{S}}/P_{\text{H}_2}$, versus reciprocal temperature (Figure 2). The equilibrium concentration of H_2S in hydrogen over Ni_3S_2 is approximately 30 ppm at 573 K, a typical methanation temperature. Thus, poisoning by H_2S in synthesis gas mixtures containing less than 30 ppm H_2S does not necessarily involve the formation of a bulk sulfide phase. Since poisoning of Ni catalysts is known to occur at much lower $\text{H}_2\text{S}/\text{H}_2$ pressure ratios, a surface phase involving adsorbed sulfur must be responsible and the heat of formation of this phase must be higher in absolute value than that of bulk Ni_3S_2 ($\Delta H_f^0 = -47$ kcal/mol).

Iron forms a number of sulfide phases,⁵ as shown in Figure 3. FeS is the most stable phase at 573 K, with $\Delta H_f^0 = -22$ kcal/mol. For the Fe-S system, the thermodynamic data⁴ shown in Figure 4 predict at equilibrium $P_{\text{H}_2\text{S}}/P_{\text{H}_2} = 6$ ppm at 573 K. For the Cu-S system, Cu_2S is the most stable⁵ phase with $P_{\text{H}_2\text{S}}/P_{\text{H}_2} = 4$ ppm at 500 K ($\Delta H_f^0 = -20$ kcal/mol)⁴, as shown in Figure 5.

H_2S Adsorption/Desorption

Chemisorption of sulfur may involve a number of steps, e.g., reversible molecular adsorption, dissociation or association, reconstruction or adsorbed sulfur into a two-dimensional compound, and incorporation into the bulk as a dissolved atom or ion or as a precipitated sulfide phase. Such process steps are illustrated by Figure 6 for H_2S adsorption on a transition metal (Me).

The evidence⁶⁻¹¹ suggests that H_2S completely dissociates on adsorption on nickel surfaces even at temperatures as low as 175 K. Isotopic (D_2) exchange experiments⁶ suggest that bound HS is an intermediate during dissociative adsorption. The coverage approaches the ratio S:Ni = 1:2 for long exposure to H_2S with the nickel surface

at 250 K or below. At temperatures higher than 300 K, incorporation of adsorbed sulfur into the bulk was observed on evaporated nickel films, with an initial activation energy at 7 kcal/mol.⁶

Hydrogen sulfide also completely dissociates on iron surfaces at low temperatures,¹² and incorporation proceeds at temperatures as low as 193 K. Diffusion through a sulfide layer limits the rate of incorporation of sulfur on nickel films.⁶ Diffusional transport appears to control the growth of bulk sulfide layers in many transition metals, except in iron, in which dissociation at the surface was reported at the slow step.¹² Rates of sulfur incorporation follow the order $\text{Fe}^{12} > \text{Ni}^6 > \text{Pd}^1, \text{Ag}^6 > \text{Pt}^6$.

The rates of adsorption of H_2S on metals are very rapid and have been studied in detail only for single crystal surfaces of copper. Figure 7(a,b) shows the coverage of adsorbed sulfur on $\text{Cu}(110)^{13}$ and $\text{Cu}(001),^{14}$ respectively, as a function of H_2S exposure. The probability of adsorption per incident H_2S molecule was constant (and approximately unity) for both surfaces until a fractional coverage with sulfur atoms corresponding to $\theta = 1/2$ was reached, presumably saturation coverage. Further slow adsorption was observed at 295 K accompanied by reconstruction of the adsorbed layer. This process is discussed further below.

The high and constant sticking probability for H_2S adsorption on copper suggests that there is no barrier to adsorption and dissociation until saturation coverage is attained. The constant probability of adsorption implies that a weakly bound adsorbed "precursor" is involved in the adsorption/dissociation sequence. A most likely precursor would be molecularly-adsorbed H_2S , as indicated in Figure 6. Weakly chemisorbed or physisorbed H_2S would have time to move over the surface and find a dissociation site before desorbing. Some weakly bound H_2S was observed

on Ni and Fe films at 183 K^{6,12} so we might expect a similar H₂S adsorption behavior for Ni and Fe as for Cu.

The rapid rates of adsorption and dissociation of H₂S on Ni, Fe, and Cu suggest that the rate of sulfur poisoning of these clean or hydrogen-covered metal surfaces is not limited by reaction at the surface. In other words, the energy barriers to adsorption, surface diffusion, and dissociation are sufficiently low to allow rapid reaction even at room temperature. As a result, the coverage of adsorbed sulfur on these metal surfaces will be controlled in practical terms by equilibrium thermodynamics.

Surface Structures

Recent advances in surface-sensitive techniques, such as low energy electron diffraction (LEED) and Auger electron spectroscopy (AES), allow detailed analysis of the geometric structure of crystal surfaces and adsorbed atoms. This experimental approach is best illustrated by the study of adsorbed sulfur on single crystal surfaces of nickel.

The electron diffraction patterns of sulfur adsorbed on Ni(001)^{15,16} at 300 K are P(2x2) at $\theta \leq 1/4$, and C(2x2) from $1.4 < \theta < 1/2$ (a monolayer is considered to represent 1.61×10^{19} S atoms/m²). The LEED patterns and proposed two-dimensional models are shown in Figure 8. The measured coverages¹⁵ for P(2x2) (21.3 ng/cm²) and C(2x2) (42.9 ng/cm²) were in good agreement with the proposed structures. No reconstruction of the C(2x2) pattern was observed on further exposure and heating; however, some faceting of the crystal face was noted.¹⁵

On the Ni(111)^{15,16,17} and Ni(110)¹⁵ planes, the adsorption of sulfur exhibited more complicated patterns. On Ni(111) at room temperature, P(2x2) structures were formed at $\theta \leq 1/4$. [On Ni(111), one monolayer equals 1.86×10^{19} atoms/m².] This structure transformed

into a $\sqrt{3} \times \sqrt{3} R 30^\circ$ pattern at higher coverage for $\theta \leq 1/3$, as shown in Figure 9. At still higher coverage and higher temperatures, reconstruction of the surface layer is observed. The complex $\sqrt{39} \times \sqrt{39}$ pattern was attributed to the reconstruction of the outermost layer into a slightly distorted Ni(001) P(2x2) sulfur overlayer on the Ni(111) substrate.¹⁶ Other, more complicated patterns were attributed to C(2x2) sulfur overlayers on the Ni(111) substrate.¹⁶ The three-dimensional structures of the complex sulfurized Ni(111) surfaces have not been determined, but clearly reconstruction occurs on Ni(111) at high sulfur coverage.

On Ni(110), initial S adsorption produced C(2x2) patterns, which gradually transformed into a P(3x2) pattern with long-range order.¹⁵ The P(3x2) pattern has been interpreted to represent a reconstructed sulfide layer.

The results of intensity analysis of the LEED patterns for the Ni(001) C(2x2), Ni(110) C(2x2), and Ni(111) P(2x2) adsorbed sulfur structures¹⁸ are shown in Figure 10. The P(2x2)¹⁹ local bonding structure on Ni(001) was found to be the same as the C(2x2) structure on Ni(001). Sulfur adatoms occupy the sites possessing maximum nearest neighbor coordination with nickel atoms. The Ni-S bond length was $2.18 \pm .06 \text{ \AA}$ for Ni(001) and (110) and $2.02 \pm 0.06 \text{ \AA}$ for Ni(111). These distances are shorter than the Ni-S nearest neighbor distance in Ni_3S_2 ²⁰ (2.28 \AA), but comparable to that of NiS.

The LEED patterns of sulfur adsorbed on iron and copper exhibit qualitative features similar to those of nickel. On Fe(001) at low coverage, the C(2x2) pattern appears; it is stable up to 773 K.²¹ At high sulfur coverage, the surface slowly transforms through a series of coincidence lattice structures with little net increase in coverage. These structures have been interpreted^{22,23} as narrowing regions of C(2x2) phases with dense close-packed boundaries and S atoms located

at sites with a coordination number of four. On Cu(001), the low coverage pattern is C(2x2),²⁴ although P(2x1)¹⁴ has been reported at high coverage. On Cu(111) the stable structure²⁴ is $\sqrt{3} \times \sqrt{3} R 30^\circ$. On Cu(110)^{24,13} the C(2x2) pattern is favored at low coverage with beam splitting occurring at 1/2 monolayer. With approximately 30% additional coverage (to 0.65 monolayer), a slow reconstruction to a P(3x2) sulfide layer is noted.

The LEED results are summarized in Table I. In general, the (111) (110) and (001) faces of Ni, Fe, and Cu form high coordination structures at sulfur surface coverage of 1/4 to 1/2 monolayer. Additional H₂S exposure often causes a slow reconstruction into a surface compound with little additional S uptake. As shown in Table II, the saturation coverage of chemisorbed sulfur on various nickel surface planes is nearly independent of original surface atom density. The S coverage was $0.82 \pm 0.04 \times 10^{19}$ atoms/m² for planes with surface Ni densities from 1.7 to 0.7×10^{19} atoms/m², suggesting that the surface reconstructs into a surface compound of similar composition regardless of the substrate geometry.

Thermodynamics

Thermodynamic data on heats of adsorption and heats of formation of sulfur chemisorbed on transition metals are sparse. The best data have been obtained for silver surfaces. The adsorption isotherms for sulfur chemisorbed on silver give evidence of a surface phase transition, i.e., the precipitation of "islands" of a surface compound. Figure 11 shows the isotherms for reversible sulfur adsorption²⁵ single crystal surface planes. The sharp increase in coverage for small increases in the H₂S/H₂ partial pressure ratio on Ag(001) and (111) may be due to reconstruction or phase transition to surface compounds. The Ag(110) surface shows an isotherm similar to the Langmuir model expected for

simple chemisorption. In Figure 12 the equilibrium sulfur activity is plotted for bulk Ag_2S^4 and for three surface orientations at one-half saturation coverage.²⁴ The equilibrium curves for the (111) and (001) surface orientation overlap and intercept the (111) curve at high temperatures. Apparently, the (110) surface binds sulfur more tightly and does not reconstruct except at temperatures greater than 773 K where the surface compound may be more stable. LEED data for the S/Ag system are not available.

Reversible sulfur adsorption on nickel is examined in Figure 2 which includes data for polycrystalline nickel foil¹⁵ and nickel supported on Al_2O_3 .²⁶ The data points were selected at sulfur coverage equal to 90% of the maximum observed coverage. Transition to the two-dimensional compound was observed in LEED experiments¹⁰ at $\theta > 1/2$. The degree of uncertainty of the data makes it difficult to apply a Van't Hoff equilibrium analysis. However, the entropy of the adsorbed layer can be estimated for 1/4 monolayer coverage assuming applicability of the Langmuir-Hinshelwood adsorption isotherm. The net entropy change is equal to the difference in entropy of H_2 and H_2S plus the vibrational entropy of adsorbed S atoms plus the net change in vibrational entropy of nickel atoms at the surface due to S adsorption. The vibrational entropies of the surface atoms can be approximated as three equal mode harmonic oscillators with frequencies defined by surface Debye temperatures. The surface Debye temperature at C(2x2) chemisorbed sulfur on Ni(001) is taken as 325 K²⁷ versus 220 K for the clean surface.²⁸ The net ΔS for adsorption ≈ 12.7 cal/K-mol at 1000 K. The estimated value of ΔS for adsorption is close to $\Delta S = 9.4$ cal/K-mol for the reaction of hydrogen with Ni_3S_2 per mole of sulfur. Thus, a Van't Hoff analysis of the equilibrium over chemisorbed sulfur should intercept the $\log_{10} \frac{P_{\text{H}_2\text{S}}}{P_{\text{H}_2}}$ of Figure 2 at about the same point as Ni_3S_2 . The dashed

lines in Figure 2 represent equilibrium lines for chemisorbed sulfur with heat of reactions 5, 10, 15, and 20 kcal/mol more exothermic than the heat of reaction of Ni_3S_2 per mole sulfur. Based on the location of the available experimental data^{15,26} at high temperatures, ΔH_{ads} of sulfur is 10 to 15 kcal/mol more exothermic than the heat of formation of Ni_3S_2 . These results indicate that it is difficult to remove chemisorbed sulfur from nickel by reaction with hydrogen at temperatures below < 900 K.

We were unable to find data concerning reversible sulfur chemisorption on iron. However, an upper limit has been estimated from experiments on removal of sulfur adsorbed on an ammonia synthesis catalyst²⁹ by reaction with hydrogen. The catalyst could not be regenerated in 1 atm H_2 at 893 K for 1000 hours. This result suggests that $\frac{P_{\text{H}_2\text{S}}}{P_{\text{H}_2}} \leq 10^{-9} \pm 10^{-1}$. This point is plotted in Figure 4. Again, taking ΔS for adsorption equal to ΔS reaction for the most stable sulfide phase, one estimates $\Delta H_{\text{ads}} = -33$ kcal/mol.

The literature reports only a single data point for reversible chemisorption of sulfur on copper.²¹ Based on the same entropy value as Cu_2S , one finds $\Delta H_{\text{ads}} \approx -16$ kcal/mol.

The results of the sparse thermodynamic data for sulfur chemisorption on Ag, Ni, Fe, and Cu all indicate that chemisorbed sulfur is far more stable than the bulk sulfides. Table III summarizes these results, where E_b is the binding energy at 1000 K of a sulfur atom at the surface or in the most stable bulk sulfide. The Table III results were obtained assuming that ΔS for chemisorption equals ΔS of the most stable sulfide, except for the silver system where more reliable data were available. For silver, the two-dimensional (reconstructed) layer apparently has lower heat of formation than chemisorbed sulfur except on the (110) plane (see Figure 12). This same trend probably exists for Ni, Fe, and Cu, except that the transition may occur at higher coverage.

Finally, we can construct a schematic isotherm for equilibrium chemisorption and precipitation of bulk material. Figure 13 represents a log-log plot of $P_{\text{H}_2\text{S}}/P_{\text{H}_2}$ versus sulfur coverage for a hypothetical 40 Å Ni catalyst particle at 573 K. A tentative exaggerated two-dimensional phase transition is included in the adsorption isotherm. Such a phase transition on metal surfaces is suggested by the S/Ag(001), Ag(111) adsorption system,²⁵ the H₂S sticking probability curve for Cu(001)¹⁴ and Cu(110)¹³, Ni^{15,16} and Cu²⁴ LEED experiments, and the 645°C isotherm on supported nickel.²⁶ For completeness, several bulk sulfide phase transitions and condensation of molten sulfur are also included.

Chemical Properties of Sulfur-Poisoned Catalysts

Unfortunately, most poisoning studies involving sulfur were conducted with $P_{\text{H}_2\text{S}}/P_{\text{H}_2}$ (or equivalent sulfur activity) > 1 ppm at 573 K. Under these conditions, rather complete poisoning and surface reconstruction would be expected. During prolonged poisoning studies in integral flow reactors, hydrogen sulfide is generally observed to pass through a nickel methanation catalyst bed in a wavefront with saturation behind the wave. The methanation activity was limited to the remaining sulfur-free surface.

The effect of sulfur poisoning on methanation catalysts has been studied in a steady flow reactor with 1 to 10 ppm H₂S added to the reactant stream.³⁰ Generally, the methanation activity of various nickel catalysts decreased 2 to 3 orders of magnitude at 325 K, with a decline in selectivity for CH₄ relative to higher molecular-weight hydrocarbons. Similar behavior was observed in a commercial methanation reactor³¹ with a nickel catalyst. Three ppm H₂S in the inlet stream caused a large decrease in activity; 0.3 ppm H₂S caused an order of magnitude decrease in activity with a significant loss in selectivity after maximum sulfur

uptake. Decreased activity and increasing molecular weight product has also been noted for a Ni-Co Fischer-Tropsch catalyst.³²

Since chemisorbed sulfur prefers high coordination sites, e.g., C(2x2) on (001) fcc metals, sulfur may readily poison reactions that require relatively weakly bound intermediates at such sites. As an example, adsorbed carbon forms a C(2x2) LEED pattern³³ on Ni(001) and presumably could be displaced by sulfur. A brief AES experiment has shown the conversion of "carbide" carbon adsorbed on a nickel foil to a graphite-like form upon sulfur adsorption at 550 K.³⁴ CO adsorbs on Ni(001), forming a C(2x2) structure at 1/2 monolayer.³⁵ At higher CO coverage, the C(2x2) structure breaks down and the binding energy decreases approximately 6 kcal/mol. Sulfur adsorption tends to block strongly bound CO adsorption sites but may allow weakly bound CO to adsorb, as observed by ir spectroscopy.^{36,37} Reactions such as methanation, which require C-O bond breaking, would be poisoned by sulfur adsorption, because the C-O bond would be strengthened as the metal-CO bond weakens, and because adsorbed sulfur is expected to compete with C or any CH_x adsorbate for high coordination sites.

Regeneration

A measure of the degree of regeneration of sulfur-poisoned Ni, Fe or Cu catalysts by reaction with H_2 may be obtained from thermodynamic considerations. For Ni at 825 K, the equilibrium pressure ratio of H_2S to H_2 is less than $< 10^{-7}$, so that a considerable amount of H_2 would be required to remove the sulfur contaminant from the surface of the catalyst. At temperatures at which the H_2S concentration approaches 100 ppm, the problem of catalyst sintering may become severe.

Regeneration by reaction of adsorbed sulfur with O_2 or H_2O may be considered. An attempt to remove surface sulfur from a $\text{Ni}/\text{Al}_2\text{O}_3$ catalyst

using H_2O vapor and H_2O/H_2 mixtures was unsuccessful.³⁸ Oxidation of surface sulfur to SO_2 by reaction with O_2 is thermodynamically favorable, but less favorable than the formation of nickel oxide.⁴ Furthermore, SO_2 is known to oxidize (and presumably sulfidize) nickel.¹ Oxidized Ni grows primarily by diffusion of Ni^{++} through the oxide layer³⁹ and could conceivably bury the sulfur at the oxide/metal interface. Subsequent reduction with H_2 could simply restore the sulfur layer. In addition, catalyst sintering may accompany exposure of a metal catalyst to oxygen at elevated temperatures. Nevertheless, at room temperature oxygen apparently can displace sulfur adsorbed on Ni(111).⁴⁰ Although regeneration of a sulfur poisoned catalyst by oxygen treatment has promise, this method may not be successful in practice.

Conclusions

- Sulfur chemisorption on Ni, Fe, and Cu has a considerable exothermic heat of surface segregation with respect to the most stable bulk sulfide, so that catalyst poisoning can occur at H_2S concentrations well below the equilibrium concentration of bulk sulfides.
- The H_2S adsorption and dissociation rates on Ni and Fe are very high even at room temperature.
- Ni and Fe readily incorporate sulfur as bulk sulfides at 300 K, provided the sulfur activity is above equilibrium values.
- Adsorbed sulfur prefers high coordination sites, thereby preempting sites required by methanation intermediates.
- As the activity of adsorbed sulfur increases, reconstruction can occur, creating a surface compound, a precursor to bulk sulfide.

- The coverage of the reconstructed surface compound is nearly independent of substrate crystallographic orientation.

REFERENCES

1. A. Huss, R. M. Gould and J. R. Katzer (to be published).
2. G. E. Haddeland, "Process Economics Program Report No. 43," p. 49, Stanford Research Institute, Menlo Park, California, 1968.
3. R. P. Elliott, "Constitution of Binary Alloys, First Supplement, McGraw Hill, New York, 1965.
4. I. Barin, O. Knacke, "Thermochemical Properties of Inorganic Substances," Springer-Verlag, New York, 1973.
5. M. Hansen, "Constitution of Binary Alloys," 2nd ed., McGraw-Hill, New York, 1958.
6. J. M. Saleh, C. Kemball, and M. W. Roberts, Trans. Faraday Soc. 57, 1771 (1961).
7. I. E. Den Besten and P. W. Selwood, J. Catal. 1, 93 (1962).
8. G. Martin and B. Imelik, Surf. Sci. 42, 157 (1974).
9. A. Rudajevova, V. Pacer, and A. Regner, Coll. Czech. Chem. Commun. 38, 2566 (1973).
10. I. Szymerska and W. Palczewska, Roczniki Chemii 45, 435 (1971).
11. J. C. Muller and R. Gibert, Bull. Soc. Chim. France 1967, 2129.
12. M. W. Roberts and J.R.H. Ross, Trans. Faraday Soc. 62, 2301 (1966).
13. H. P. Bonzel, Surf. Sci. 27, 387 (1971).
14. R. W. Joyner, C. S. McKee, and M. W. Roberts, Surf. Sci. 27, 279 (1971).
15. M. Perdercau and J. Oudar, Surf. Sci. 20, 80 (1970).
16. T. Edmonds, J. J. McCarroll, and R. C. Pitkethly, Nederlands Tijdschrift voor Vacuumtechniek 8, 162 (1970).

17. T. Edmonds, J. J. McCarroll, and R. C. Pitkethly, *J. Vac. Sci. Tech.* 8, 68 (1971).
18. J. E. Demuth, D. W. Jepsen, and P. M. Marcus, *Phys. Rev. Lett.* 32, 1182 (1974).
19. M. Van Hove and S. Y. Tong, *J. Vac. Sci. Tech.* 12, 230, (1975).
20. R.W.G. Wyckoff, "Crystal Structures" 2nd ed., Vol. 2, Wiley New York, 1964.
21. J. Bénard, *Catal. Rev.* 3, 93 (1969).
22. M. Huber and J. Oudar, *Surf. Sci.* 47, 605 (1975).
23. J. P. Biberian, M. Huber, *Surf. Sci.* 55, 259 (1976).
24. J. L. Domange and J. Oudar, *Surf. Sci.* 11, 124 (1968).
25. J. Bénard, J. Oudar, and F. Cabané-Brouty, *Surf. Sci.* 3, 359 (1965).
26. J. R. Rostrup-Nielsen, *J. Catal.* 11, 220 (1968).
27. J. E. Demuth, D. W. Jepsen, and P. M. Marcus, *Phys. Rev. Lett.* 31, 540 (1973).
28. A. U. McRae, *Surf. Sci.* 2, 512 (1964).
29. R. Brill, H. Schaefer, and G. Zimmermann, *Berichte Bunsengesellschaft* 72, 1218 (1968).
30. R. A. Dalla Betta, A. G. Piken, and M. Shelef, *J. Catal.* 40, 173 (1975).
31. L. Seglin, ed., "Methanation of Synthesis Gas," American Chemical Society, Washington, D.C., 1975.
32. H. H. Storch, N. Golumbic, and R. B. Anderson, "The Fischer Tropsch and Related Syntheses," Wiley, New York, 1951.
33. J. C. Shelton, H. R. Patil, and J. M. Blakely, *Surf. Sci.* 43, 493 (1974).
34. B. J. Wood. Semiannual Report for AGA, May 1974.
35. J. C. Tracy, *J. Chem. Phys.* 56, 2736 (1972).

36. W. Crell, H. Hobert, and B. Knappe, Z. Chem. 10, 396 (1968).
37. R. T. Rewick and H. Wise (to be published).
38. J. R. Rostrup-Nielsen, J. Catal. 21, 171 (1971).
39. O. Kubaschewski and B. E. Hopkins, "Oxidation of Metals and Alloys," Butterworths, London, 1962.
40. P. H. Holloway and J. B. Hudson, Surf. Sci. 33, 56 (1972).

FIGURE CAPTIONS

1. Nickel-Sulfur Phase Diagram
2. Nickel-Sulfur Equilibrium
3. Iron-Sulfur Phase Diagram
4. Iron-Sulfur Equilibrium
5. Copper-Sulfur Equilibrium
6. H_2S /Metal Interface
7. H_2S Adsorption
8. Surface Structures of Chemisorbed Sulfur on Ni(001)
9. Surface Structure of Chemisorbed Sulfur on Ni(111)
10. Surface Structure of Ni(110) C(2x2)-S, Ni(001) C(2x2)-S, and Ni(111) P(2x2)-S
11. Sulfur Adsorption Isotherms on Silver
12. Silver-Sulfur Equilibrium
13. Sulfur Adsorption Isotherm on Nickel at 573 K

TABLES

- I Surface Structures of Adsorbed Sulfur
- II Saturation Coverage of Surface Sulfur on Nickel at 573 K
- III Heat of Formation of Surface and Bulk Metal Sulfides at 1000 K

Table I

SURFACE STRUCTURES OF ADSORBED SULFUR

Surface	Structures*		Ref. No.
	Adsorbate	Surface Compound	
Ni(001)	P(2x2) C(2x2)	C(2x2)	15,16
Ni(111)	P(2x2) $\sqrt{3} \times \sqrt{3}$ R 30°	$\sqrt{39} \times \sqrt{39}$ $5\sqrt{3} \times 2$ $8\sqrt{3} \times 2$ $\sqrt{21} \times \sqrt{84}$	15,16,17
Ni(110)	C(2x2) split spots	P(2x2) P(4x1)	15
Fe(001)	C(2x2)	C(22x2) (18x2) (14x2) (10x2)	21,22,23
Cu(001)	C(2x2) P(2x1)	$\sqrt{17} \times \sqrt{17}$	24 14
Cu(111)	$\sqrt{3} \times \sqrt{3}$ R 30°	$\sqrt{7} \times \sqrt{7}$	24
Cu(110)	C(2x2) split spots	P(3x2)	13,24

* As determined by low energy electron diffraction (LEED)

Table II

SATURATION COVERAGE OF SURFACE
SULFUR ON NICKEL AT 873 K

Crystal Plane	Surface Concentration (ng/cm ²)	Concentration of Ni(clean) (10 ¹⁵ atom/cm ²)	Concentration of S (saturated) (10 ¹⁵ atom/cm ²)
(111)	47 ± 1	1.8	0.86
(100)	43	1.6	0.80
(110)	44.5	1.1	0.82
(210)	42	0.72	0.78
Polycrystalline	44.5	-	0.82
		Average: 0.82 ± 0.04	

Reference 21: J. Benard, *Cat. Reviews* 3, 93 (1969).

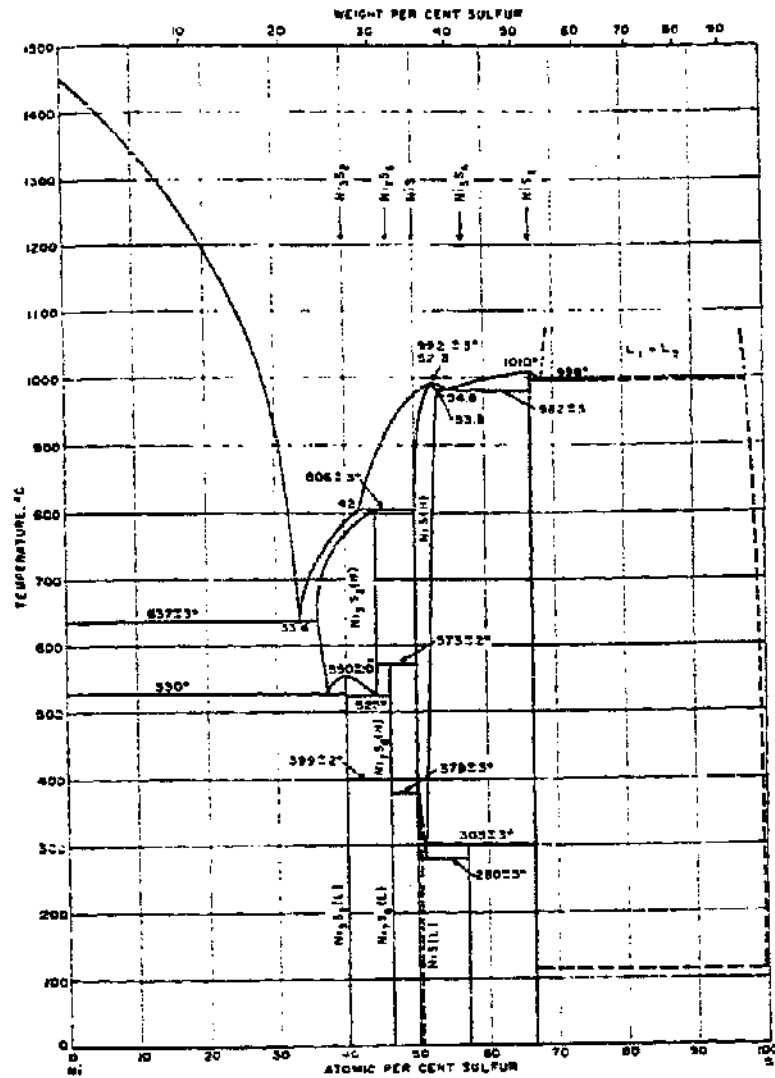
Table III

HEAT OF FORMATION OF SURFACE AND
BULK METAL SULFIDES AT 1000 K

Metal	Surface	ΔH_f^*	E_B^\dagger	Bulk Phase	E_B^\dagger	ΔH_{seg}^*
Ni	(polycryst. supported)	-32	98	Ni_3S_2	87	-11
Cu	polycryst	-19	86	Cu_2S	79	-7
Fe	supported	<-37	>103	FeS	84	<-19
Ag	(110)	-20	87	Ag_2S	67	-20
	(111), (001)	-12	78			-11

* ΔH_f , ΔH_{seg} , and E_B have units kcal per mole sulfur atoms.

† E_B represents the binding energy of monatomic sulfur (gas) to the corresponding surface or bulk phase.



SOURCE: Reference 3.

TA-350522-168

FIGURE 1 NICKEL-SULFUR PHASE DIAGRAM

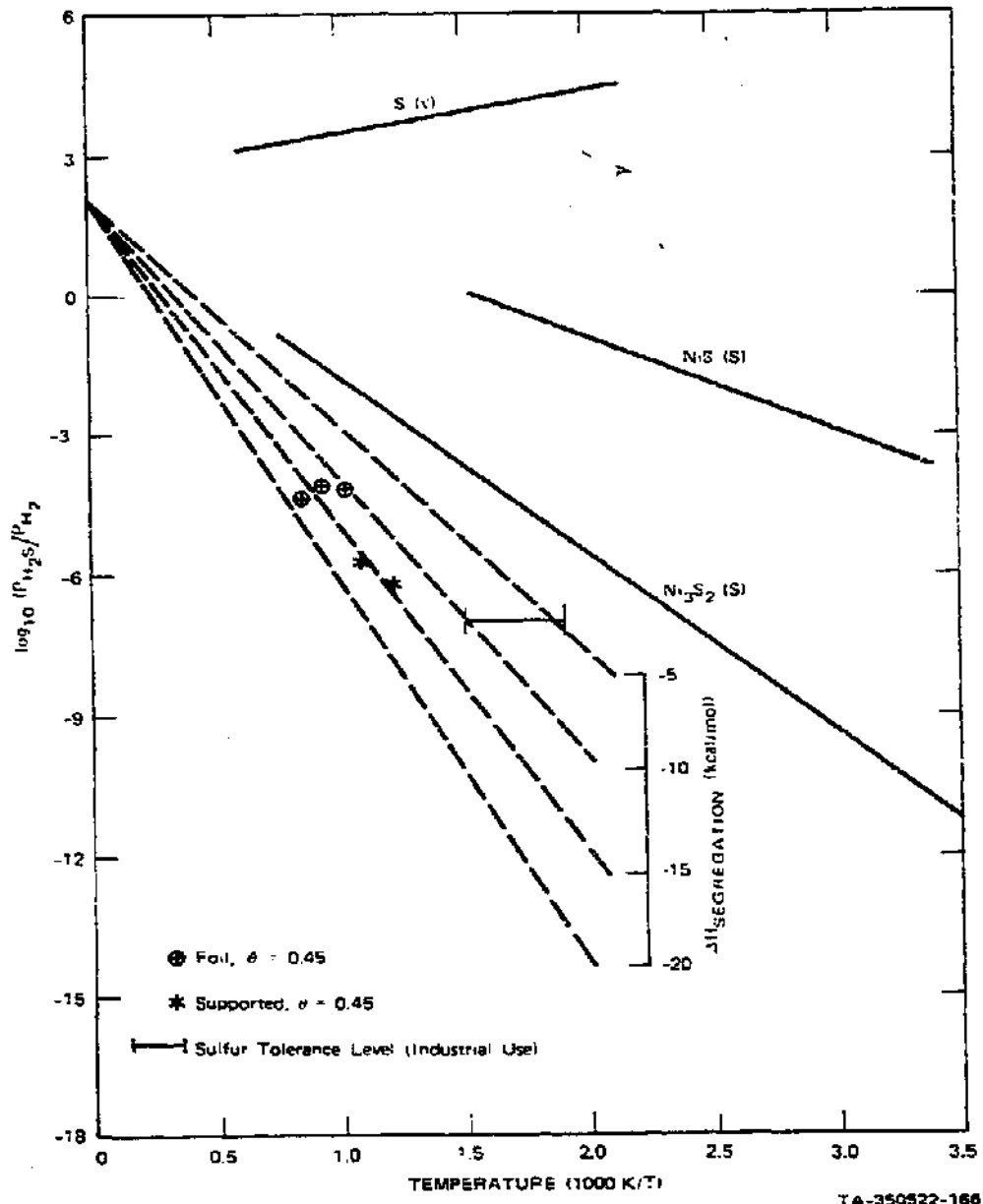


FIGURE 2 NICKEL-SULFUR EQUILIBRIUM

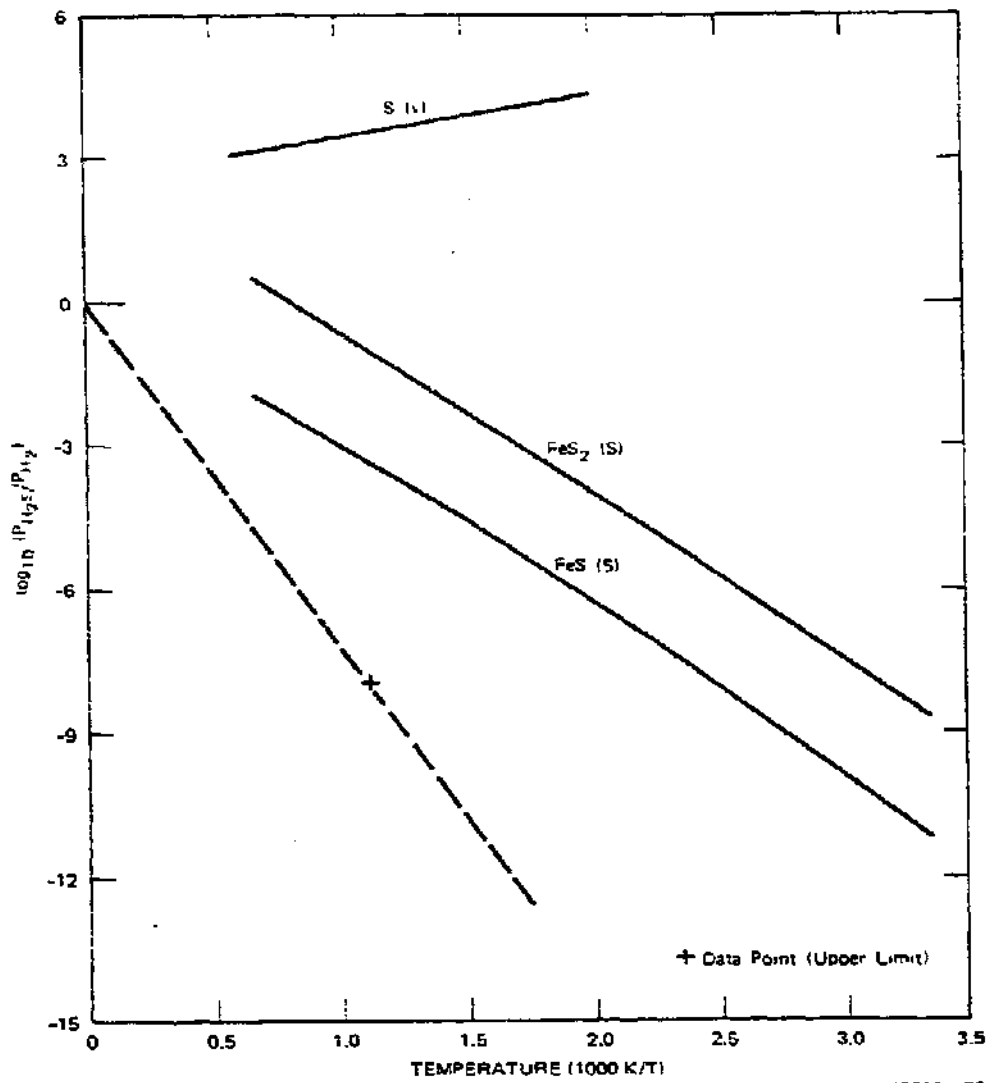


FIGURE 4 IRON-SULFUR EQUILIBRIUM

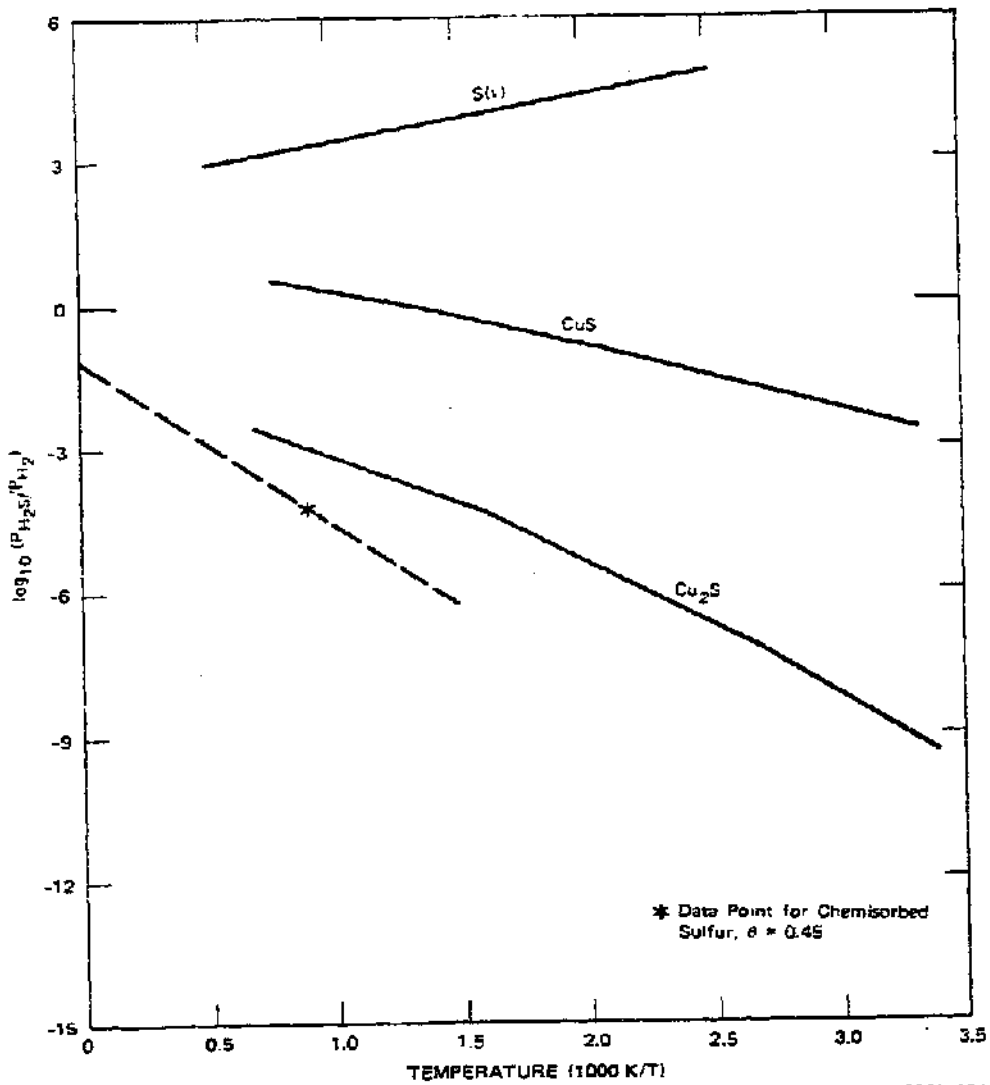
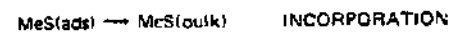
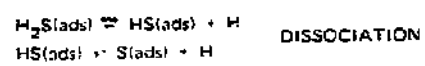
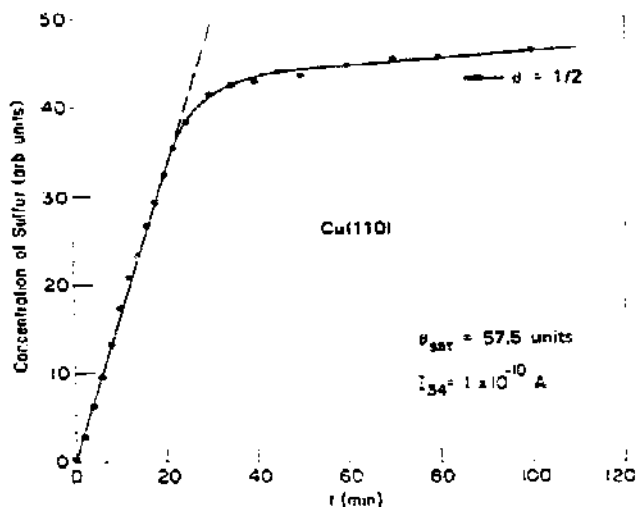


FIGURE 5 COPPER-SULFUR EQUILIBRIUM



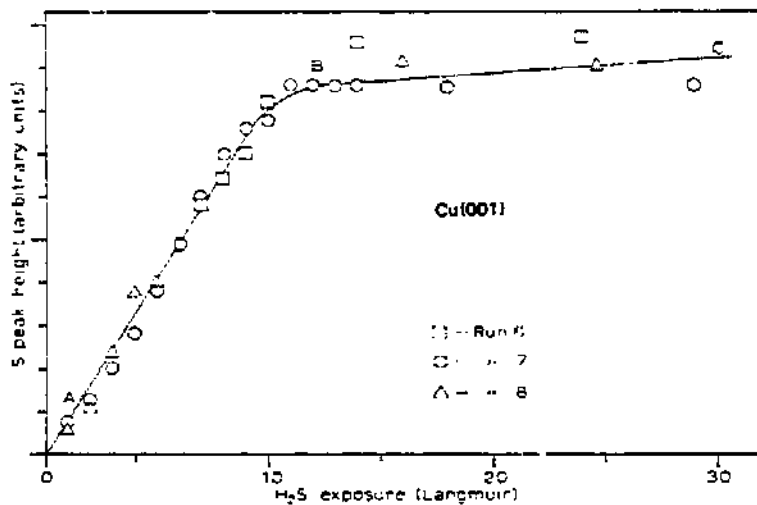
TA-350522-172

FIGURE 6 HYDROGEN SULFIDE/METAL INTERFACE



SOURCE: Reference 13.

(a) CONCENTRATION OF ADSORBED SULFUR AS A FUNCTION OF TIME AT ROOM TEMPERATURE AND CONSTANT PARTIAL PRESSURE OF H_2S



SOURCE: Reference 14.

(b) DERIVATIVE PEAK-TO-PEAK HEIGHT OF THE S (150eV) AUGER PEAK AS A FUNCTION OF THE EXPOSURE OF Cu(001) TO $H_2S(g)$ AT 295 K

TA-350522-173

FIGURE 7 HYDROGEN SULFIDE ADSORPTION ON Cu(110) AND Cu(001)

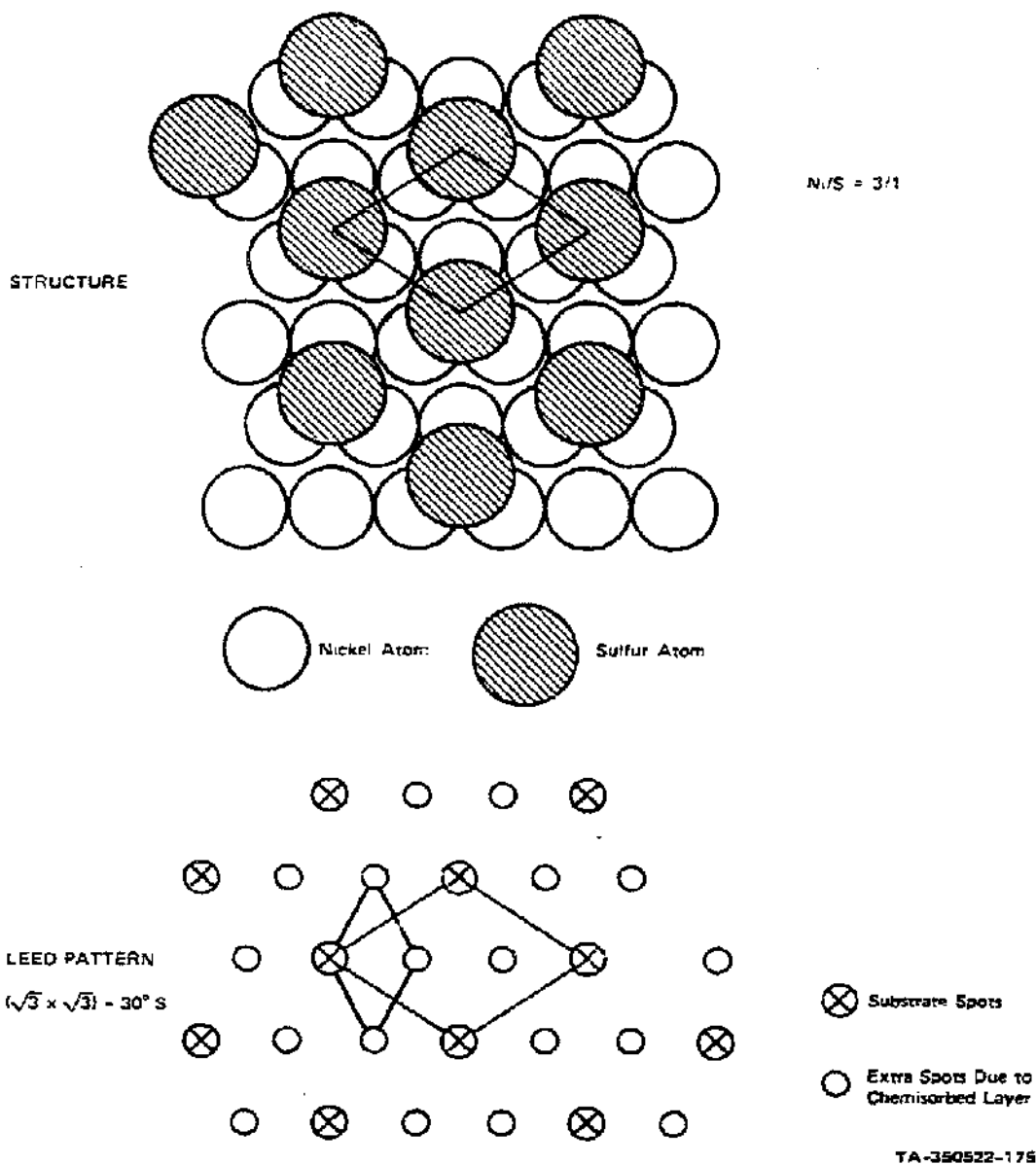
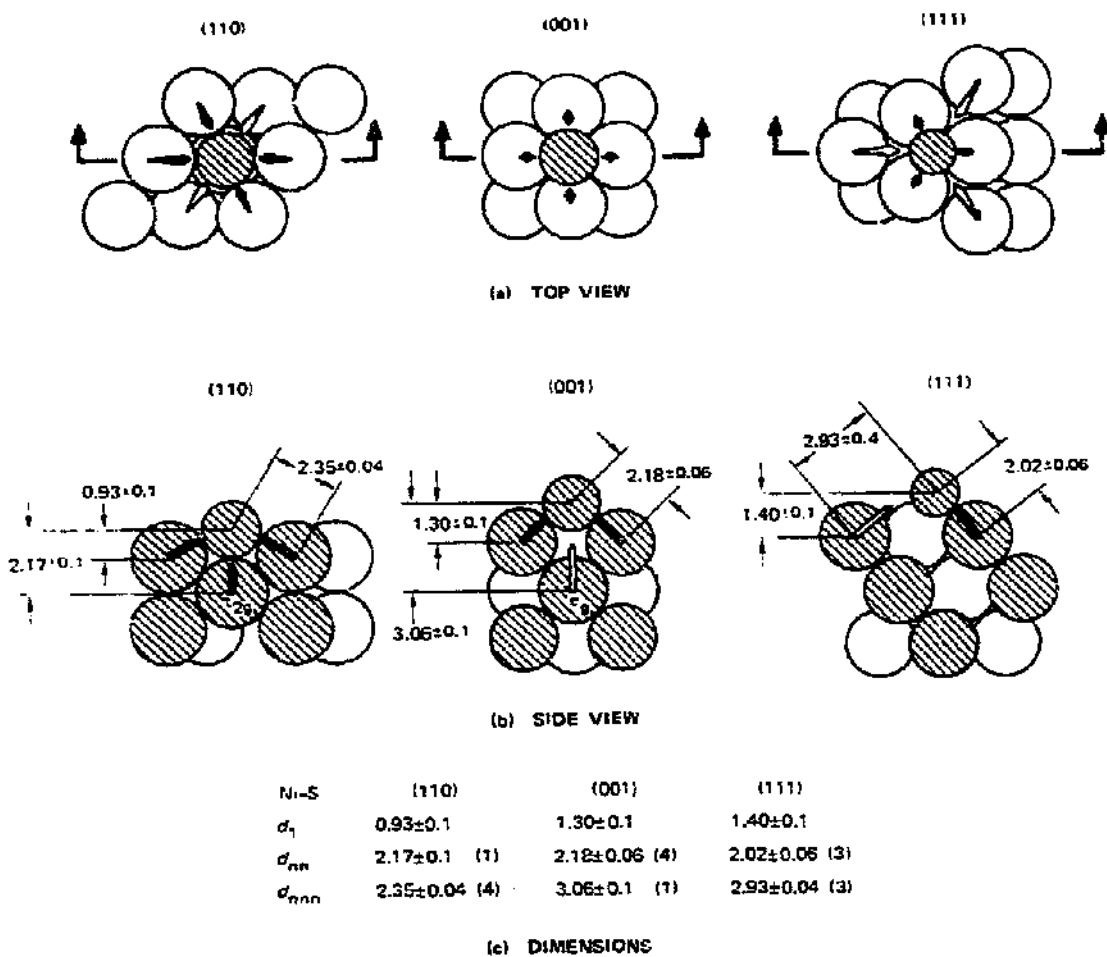


FIGURE 9 SURFACE STRUCTURE OF CHEMISORBED SULFUR ON Ni(111)



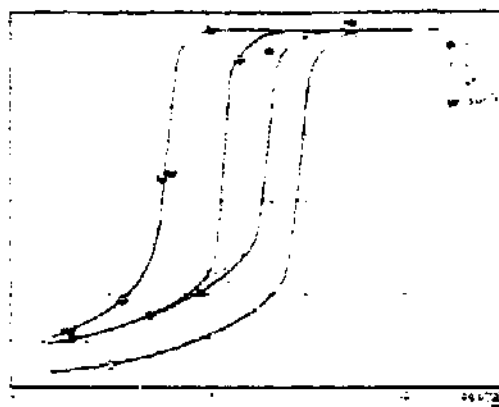
Schematic diagram showing the determined atomic bonding sites of the sulfur atoms in the $C(2 \times 2)$, $C(2 \times 2)$, and $P(2 \times 2)$ structures on the (110), (001), and (111) nickel surfaces, respectively, as viewed from (a) above the surface (top view) or (b) from a cut-away section along the horizontal direction (side view). The preferred adsorption site on the (111) surface is the threefold hollow site which does not have another nickel atom below [site 1]. The filled and open arrows represent e_g and t_{2g} molecular orbitals of the substrate, respectively.

SOURCE: Reference 18.

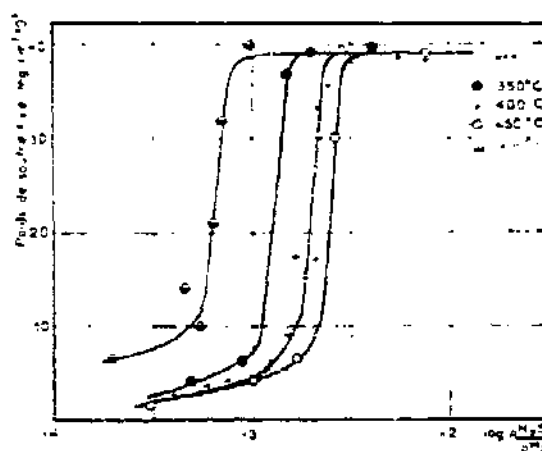
TA-350522-176

FIGURE 10 SURFACE STRUCTURE OF Ni(110) $C(2 \times 2)$ -S, Ni(001) $C(2 \times 2)$ -S, AND Ni(111) $P(2 \times 2)$ -S

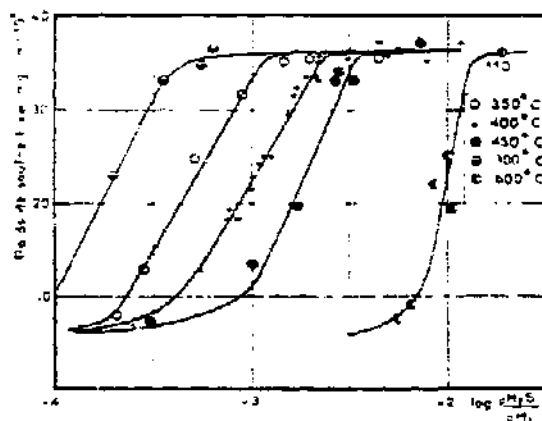
(a) Ag(100)



(b) Ag(111)



(c) Ag(110)



SOURCE: Reference 25.

TA-350522-177

FIGURE 11 SULFUR ADSORPTION ISOTHERMS ON SILVER

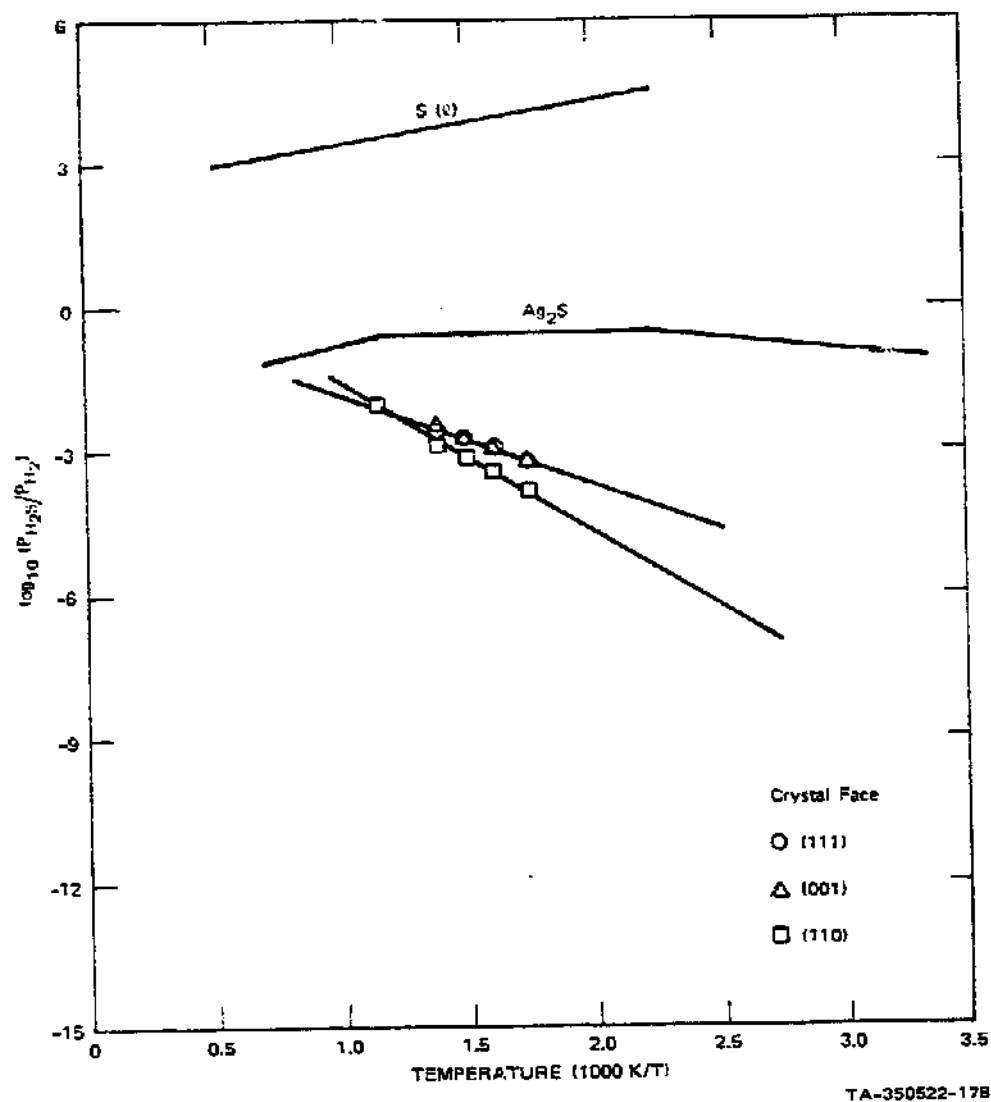


FIGURE 12 SILVER-SULFUR EQUILIBRIUM

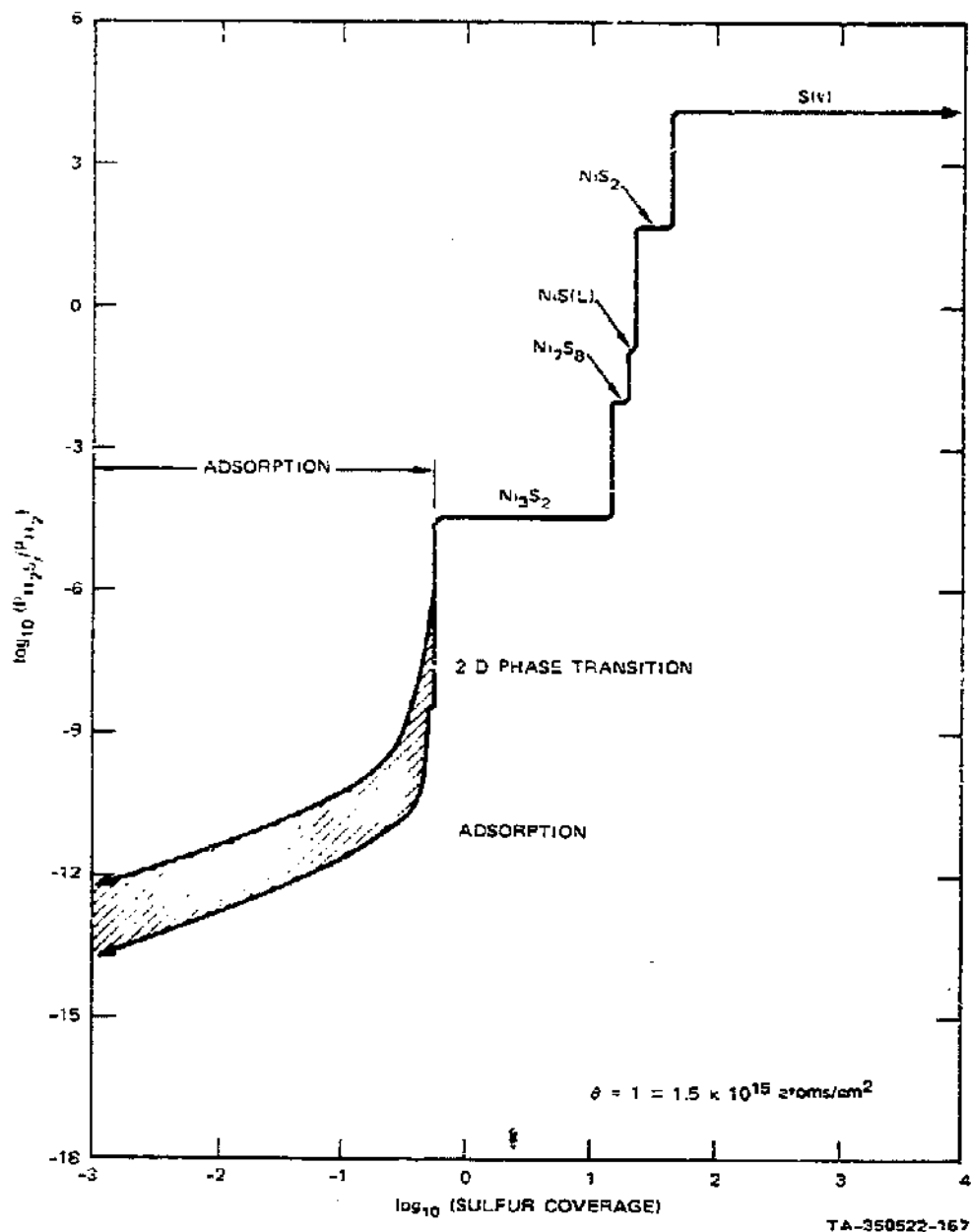


FIGURE 13 SCHEMATIC ISOTHERM--SULFUR COVERAGE VERSUS SULFUR ACTIVITY FOR 46 Å NICKEL PARTICLES AT 573 K